NASA Contractor Report 3070

Numerical Computation of Transonic Flows by Finite-Element and Finite-Difference Methods

M. M. Hafez, L. C. Wellford,
C. L. Merkle, and E. M. Murman

NASA

NASA Contractor Report 3070

Numerical Computation of Transonic Flows by Finite-Element and Finite-Difference Methods

M. M. Hafez
Flow Research Company, Kent, Washington

L. C. Wellford
University of Southern California, Los Angeles, California

C. L. Merkle and E. M. Murman
Flow Research Company, Kent, Washington

TABLE OF CONTENTS

LIST OF FIGURES

LIST OF FIGURES

(Continued)

SUMMARY

This report contains our studies on applications of the finite-element approach to transonic flow calculations, and it includes comparisons between different discretization techniques of the differential equations and boundary conditions. Transonic flow calculations can be divided into two main categories: type-sensitive methods and type-insensitive methods. Finite-element analogs of Murman's mixed-type finite-difference operators for small-disturbance formulations are constructed, with different strategies used in the subsonic and supersonic regions. In the supersonic region, no upstream effect is allowed; blending elements are introduced between different regions. On the other hand, as an example of type-insensitive methods, the time-dependent (unsteady) approach (using finite differences in time, finite elements in space) is examined. The elliptic methods, where the transonic equation is cast into Poisson's form with the nonlinear terms as a driving force, provide another example. The report is concluded with a general shock-fitting procedure based on discontinuous shape functions and with possible extensions to full potential equations.

INTRODUCTION

Computations of steady transonic flow can be formulated in terms of either the Euler equations or the velocity potential equation; but, regardless of which formulation is chosen, these computations generally rely on one of two basic iterative procedures. The first procedure involves integrating a set of hyperbolic equations (in time) until a steady state is reached, while the second approach makes use of relaxation techniques.

The hyperbolic procedure is frequently formulated in terms of the complete unsteady Euler equations, but other hyperbolic forms of the equations of motion have also been used. The hyperbolic procedure is attractive because a converged solution, which includes both subsonic and supersonic regions, can be obtained without making any explicit consideration of the mixed character of the flow field. Unfortunately, the convergence to the steady state has proved to be quite slow.

By contrast, the relaxation procedures cannot produce converged solutions unless special local (spatial) discretization procedures that account for the mixed elliptic-hyperbolic nature of the flow field are used. When the local character of the flow field is properly accounted for, however, the relaxation procedures converge much faster than the hyperbolic ones. The choice of the most appropriate type of spatial discretization must take into account their differences.

Solutions of the Euler equations in the transonic regime have been obtained by means of standard finite-difference procedures (based on the Lax-Wendroff or the McCormack schemes) as well as finite-volume techniques. Solutions of the velocity potential equation have generally relied on the use

of type-dependent, finite-difference schemes cf the kind first introduced to numerical transonic flow calculations by Murman and Cole (ref. 1). Recently, accelerated iteration procedures for finite-difference calculations using fast Poisson solvers (elliptic methods) proved to be very efficient. Martin and Lomax (ref. 2) used elliptic methods, in the form of a system of first-order equations, for cases of small disturbance, while Jameson (ref. 3) solved the full potential equation.

In this report, we examine the application of the finite-element approach to transonic flow calculations. We consider hyperbolic, mixed-type, and elliptic methods. The appeal of finite-element procedures is twofold. First, finite-element procedures are capable of accurately and efficiently enforcing boundary conditions, even when the boundaries are geometrically complex. (The application of boundary conditions in finite-difference schemes becomes very difficult when the boundaries are complex in shape.) Second, finite-element procedures reduce the number of grid points (or elements) required to achieve a solution of a desired accuracy through the use of efficient, higher-order shape functions or mixed finite-element methods. We note that, although both of these advantages are important in two-dimensional flows (with which we are concerned in this report), they become crucial in three-dimensional calculations.

We have carried over from finite-difference methods as much understanding of numerical transonic techniques as possible. More specifically, we have made the basic assumption that techniques that are successful in transonic flow regimes when using finite-difference methods should also be successful when using finite-element techniques, and likewise for techniques that fail. As a result, our primary emphasis has been on solving the small-disturbance equation,

not the full velocity potential equation. Furthermore, we have been satisfied with enforcing boundary conditions on a straight line (in accordance with small-disturbance theory). The use of finite-element procedures on this simplified problem as an end in itself is not justified; finite-difference methods are undoubtedly better suited to the small-disturbance problem. Nevertheless, we believe that the feasibility of developing finite-element procedures that are capable of handling mixed, elliptic-hyperbolic flow fields can best be demonstrated in this simpler environment. Extension to the more complicated problems for which finite-element methods are better suited should be simplified after the small-disturbance problem has been completed.

Much of our present effort, therefore, has been spent on solving the small-disturbance equation in a rectangular domain with simplified boundary conditions, by means of rectangular elements and linear shape functions. This simplification not only makes the finite-element procedure easier to apply, but also brings it parallel with finite-difference procedures, which have proven to be successful in this simplified problem.

From this "jumping-off" point, we proceed to higher-order shape functions with a parallel review of higher-order-accurate, finite-difference procedures so that effects that are related to improved accuracy can be separated from those that are derived from the basic differences between finite-element and finite-difference techniques. Finally, using elements with curved boundaries, we consider the solution of the full potential equation and its extension to nonrectangular domains.

One of the most prominent differences between finite differences and finite elements that persists even in the simplified problem described above is that the matrices associated with finite-element schemes are generally

4

solved by direct methods rather than by the relaxation techniques that are used in finite-difference methods. Economically, iterative techniques are usually more suitable for large, sparse matrices, whereas direct methods are more suitable for more moderately sized matrices. As noted above, the larger elements that can be used for finite elements result in matrices more moderate in size, so direct inversion is favored. Later in this report we consider whether it is more economical to relax or to invert directly a given matrix system, but we note here that there is mathematical basis for selecting one scheme over the other. For example, because of the unique properties that are transmitted to the matrix when the equation changes type (from elliptic to hyperbolic), relaxation methods could fail while direct methods would succeed. That is, the relaxation procedure might diverge even in cases where the inverse of the matrix actually exists.

One of the most important features of transonic flows is shock waves. Like finite-difference methods, shocks are either captured or fitted. In this report we discuss a general shock-fitting procedure for finite-element calculations and we use a simple version in our computations.

TRANSONIC SMALL-DISTURBANCE THEORY

The assumption of the existence of a velocity potential, along with restriction to small disturbances, greatly simplifies the transonic flow problem while, at the same time, it retains all the fundamental nonlinear, mixed-type mathematical properties that are characteristic of transonic flows. Despite its relative simplicity, the small-disturbance equation is capable of adequately describing the transonic flow field around many configurations of

practical interest, and it has been used in numerous engineering applications. In its small-disturbance form, the transonic velocity potential equation is

$$(K - \phi_x)\phi_{xx} + \phi_{yy} = 0 , \tag{1}$$

where ϕ represents the perturbation velocity potential, K represents a transonic similarity parameter, and x and y refer to a Cartesian coordinate system (see fig. 1). The boundary condition to be applied in the vicinity of the body is

$$\phi_y = f_{\pm}(x) - \alpha , \tag{2}$$

where $f_{\pm}$ represents the body shape and α signifies the angle of attack. Consistently with the small-disturbance approximation, this boundary condition may be applied on the line $y = 0$. The airfoil surface boundary condition is generally complemented by an analytic expression for the far field, which represents the combined effects of a doublet and a vortex. The formulation of the problem is summarized in figure 1.

In the small-disturbance equation, the sonic line is given by the point where $\phi_x = K$, and, by inspection of equation (1), we see that when $\phi_x = K$ (sonic condition), ϕ_{yy} vanishes. This latter condition is enforced explicitly in many numerical schemes. Once ϕ_x becomes greater than K, the equation changes type and becomes hyperbolic. In the hyperbolic (supersonic) region, the characteristic directions are

$$(dx/dy)_c^2 = \phi_x - K , \tag{3}$$

6

while the shock relations for the small-disturbance velocity potential formulation are

$$\langle K - \phi_x \rangle = - (dx/dy)_s^2 \tag{4}$$

and

$$\left(\frac{dx}{dy}\right)_s = - \frac{[\![\phi_y]\!]}{[\![\phi_x]\!]} , \tag{5}$$

where $\langle \ \ \rangle$ and $[\![\ \ ]\!]$ signify the average and the jump across the discontinuity, respectively.

Related Work on the Small-Disturbance Equation

In conjunction with our discussion of the small-disturbance equation, we mention some related work. Some of this work is related to information that can be used to understand the iterative procedure, some is concerned with developing more economical iterative procedures, and some describes appropriate limitations on the small-disturbance approximations that support the transonic small-disturbance equation.

One interesting study is the work of Sichel (ref. 4), who considered the effects of viscosity on transonic flows. In his work, Sichel used the viscous transonic equation:

$$\phi_x \phi_{xx} - \phi_{yy} = \nu \phi_{xxx} . \tag{6}$$

Although his work points out some important limitations of inviscid transonic small-disturbance theory, we wish to reference here the direct parallel between the physical viscosity term in the viscous transonic equation and the artificial (or numerical) viscosity that is used in numerical transonic flow studies. We discuss artificial viscosity in later sections.

Another work of interest is Landahl's investigation (ref. 5) of the unsteady transonic equation:

$$(K - \phi_x + \alpha\phi_t)\phi_{xx} + \phi_{yy} = \beta\phi_{xt} + \gamma\phi_{tt} \ . \tag{7}$$

This equation can be construed as representing one of the complete unsteady solution procedures described in the Introduction. A second interesting aspect of this equation, however, is the so-called low-frequency form of this equation, which is obtained by neglecting the high-frequency terms ϕ_{tt} and ϕ_t as follows:

$$(K - \phi_x)\phi_{xx} + \phi_{yy} = \beta\phi_{xt} \ . \tag{8}$$

Equation (8) is closely related to the relaxation procedure used to solve the transonic small-disturbance equation.

Finally, we should enumerate some of the limitations of the transonic small-disturbance equation. The approximations upon which the transonic small-disturbance equation are based generally break down near the leading edge of a transonic wing. Such leading edges are, for engineering reasons, generally blunt, so the flow must turn as much as 90° from its original direction. Turns of this magnitude are not allowed in small-disturbance theory. Keyfitz, Melnik,

8

and Grossman (ref. 6) have given more complete consideration of the problem of the blunt leading edge. Fortunately, ignoring the details of the leading edge region allows acceptable engineering accuracy to be achieved in the remainder of the flow field.

Sirovich and Huo (ref. 7) have tested the validity of the transonic small-disturbance equation in the vicinity of the sonic line, while Landau (ref. 8) and Guderley (ref. 9) have discussed the details of the flow in the intersection between the sonic line and the shock wave. The intersection of a normal shock wave with a curved surface has been discussed by Zierep and Oswatitsch (ref. 10), who determined the character of the solution near this singularity.

One transonic phenomenon that we do not consider in this report, but must at least mention, is the effect of viscosity in transonic flow regimes. Viscosity is important in shock-wave boundary-layer interactions and in the trailing edge region. Either of these regions can generate local-separation bubbles, which substantially alter the flow from its unseparated, inviscid state. Some specific works that discuss methods for including these viscous effects include those by Melnik and Grossman (ref. 11).

FINITE DIFFERENCES

Unsteady Approach

Magnus and Yoshihara (ref. 12) obtained numerical solutions of the Euler equation in the transonic region, using a Lax-Wendroff finite-difference scheme (with artificial viscosity) marching in time to the steady state. For small disturbances, Magnus and Yoshihara used the following hyperbolic system of equations:

$$U_t = (K - U)U_x + V_y \ , \tag{9}$$

$$V_t = -V_x + U_y \ . \tag{10}$$

The calculations were too lengthy and expensive, and, hence, this method was abandoned.

Murman's Fully Conservative Scheme

One of the most popular techniques for solving the transonic small-disturbance equation (TSDE) is Murman's fully conservative, type-dependent, finite-difference scheme, or variants of it (see ref. 13). As indicated in figure 2, Murman's scheme is characterized by four distinct operators: an elliptic operator E for subsonic regions; a hyperbolic operator H for supersonic regions; a parabolic operator P for points on (or near) the sonic line; and a shock-point operator SPO for enforcing the jump conditions across the shock. The elliptic operator is based on a second-order-accurate, central-difference formula, while the hyperbolic operator is obtained from a first-order-accurate, backward-difference representation. The remaining two operators, the parabolic operator and the shock-point operator, represent blending elements for grid points on the boundaries between elliptic and hy-perbolic regions.

The four finite-difference operators described above can be used to convert the continuous, partial differential equation (1) into a discrete system of algebraic equations which describe the behavior of the solution at a fixed set of points in the flow field. The system of equations generated by this discretization is generally solved by a line-relaxation algorithm

10

which iteratively sweeps the matrix, line-by-line, from left to right. During the relaxation process, the solution is over-relaxed $(\omega > 1)$ in the elliptic region, but in the remainder of the field it is usually mildly under-relaxed $(\omega \leq 1)$. Since this discretization scheme is only first-order accurate in the supersonic region, it is first-order accurate overall. Because of the relative simplicity of the scheme, the low accuracy can be offset by using a finely divided mesh.

We note that, in the far field, the doublet strength due to the flow around the body is given by

$$D = \iint \phi_x^2 \; dx \; dy + D_{linear} \quad . \tag{11}$$

As can be seen, the doublet strength depends on the solution itself. The double integral is generally updated at selected intervals during the iterative procedure so that when the solution converges, the far-field representation is intimately tied to the numerical solution (and conversely).[*] The use of this analytical representation of the solution far from the airfoil greatly decreases the domain included in the computation.

A series of sample calculations, which have been obtained from Murman's fully conservative scheme and which indicate the influence of various factors in the scheme on the final solution, are given in figures 3A through 3C.

---

[*]We also note that Cheng and Hafez (ref. 14) have shown that the far-field behavior near the boundary may be fitted by using a least-squares technique; thus, performing the double integration over the entire flow field is no longer necessary.

The base case, which is designated as "Case A1" in the figure, includes all the factors in the Murman scheme, as described above. Unless otherwise noted, these calculations are for a uniformly-spaced grid system in both the x and y directions, with 10 grid points on the airfoil surface, 10 points upstream of the leading edge, and 10 points downstream of the trailing edge.

The first comparison (fig. 3A) demonstrates the effect of the shock-point operator on the final results. As shown, the shock-point operator allows a much more rapid velocity change across the shock (compare Cases A1 and B1 in fig. 3B). The comparison between Cases A1 and C1 shows the effect of incorporating the far-field solution (Case A1) instead of enforcing a homogeneous boundary condition $(\phi = 0)$ at the same point (Case C1). Case D1 shows the effect of placing the leading and trailing edge points halfway between grid points, compared to the effect of placing grid points on the leading and trailing edge points. The results in figure 3C show that the apparent shape of the airfoil is altered when the positions of the leading and trailing edge points are shifted with respect to the grid system. This effect is amplified in the present case by our use of a relatively coarse grid system. Also in figure 3C, we show the effect of halving the grid size. Cases D1 and H1 show the higher degree of accuracy that can be obtained with the finer grid system.

Among other considerations that are directly related to numerical methods are those techniques concerned with accelerating Murman's relaxation solution so that convergence can be obtained more rapidly. One such approach is the use of extrapolation techniques, such as those reported by Cheng and Hafez (ref. 15) and Caughy and Jameson (ref. 16). Extrapolation techniques attempt to accelerate the painfully slow iterative procedure by obtaining numerical

12

estimates of the dominant eigenvalues in the finite-difference matrix and by using these eigenvalues to extrapolate the iteration to a level much closer to convergence. Such extrapolation techniques have exhibited time savings of a factor of 4 to 5 over the more conventional line-relaxation procedures.

A second acceleration device, which has proven very effective for finite-difference calculations, is one that replaces the nonlinear transonic equation with a Poisson equation having the nonlinear term as a right-hand-side term. The matrix corresponding to the constant-coefficient elliptic (left-hand-side) operator is then solved by a direct inversion technique. Based on this interim solution, the nonlinear (right-hand-side) term is updated, and the "fast-solver" is again employed. With this technique, convergence has been very rapid (generally less than 10 of these major iterations), provided the supersonic region is treated properly. If no special treatment is applied for the supersonic region, the procedure fails. Very impressive results (in terms of the amount of computer time required) have been reported by both Martin and Lomax and by Jameson (see refs. 2 and 3). In their studies, slightly different techniques were used for treating the supersonic region. These are discussed more fully in the following section, A Fully Conservative, Second-Order Scheme for Finite Differences.

Two additional studies that are concerned with developing more rapid computational procedures are also in progress. Ballhaus and Steger (ref. 17) and Jameson (ref. 3) are using alternating-direction implicit methods, based on an efficient matrix factorization technique for solving the Euler equations. The second approach is a multi-grid technique being developed by Brandt and South (ref. 18). This technique solves the transonic equation on a series of grid

spacings which vary from fine to coarse and fine again. The basis of this pro-
cedure is to increase the speed of the iterative relaxation process by
diminishing the error in a different segment of the frequency spectrum of the
matrix with each distinct grid system.

Another acceleration technique is the use of discrete, shock-fitting pro-
cedures, which have been reported by Cheng and Hafez and by Yu and Seebass
(see refs. 15 and 19). Shock-fitting really has no capability for increasing
the speed of the relaxation process; however, it indirectly achieves such an
improvement. Shock-fitting is really concerned with improving the spatial
discretization so that shock waves can be handled with a relatively coarse mesh
(compared to the extremely fine grid that must be used when the shock is not
fitted). The coarse grid that is used with shock-fitting decreases the amount
of computational time by reducing the number of unknowns (grid points) to be
computed.

A Fully Conservative, Second-Order Scheme for Finite Differences

As indicated in the previous section, Murman's fully conservative finite-
difference scheme is accurate only to the first order. The low accuracy occurs
because upstream effects are not allowed in the supersonic region, and, hence,
one-sided differences must be used in that region. The numerical scheme is
therefore (formally) less accurate in supersonic regions than in subsonic
regions, where central differencing is employed. To make the accuracy in the
supersonic region comparable with that in the subsonic region (thus making
the entire calculation second-order accurate), we may use either of two methods.
We can include more grid points in the computations for supersonic points, or we

can turn to a Hermitian scheme in which both ϕ and its derivatives are stored and used at each grid point.

One reason for considering a finite-element scheme is the premise that, through the use of a more accurate local representation of the solution, the total number of grid points can be decreased, and, thus, the computer storage requirements, as well as the central processor time requirements, can be reduced. Such goals are particularly urgent for three-dimensional transonic flows. With the goal of improved accuracy in mind, we consider first the requirements that are imposed on a finite-difference scheme when it is extended to higher accuracy. It seems reasonable to expect that those problems encountered in a second-order-accurate, finite-difference scheme would also be present in a finite-element scheme, so their solution should give some indication of whether a given finite-element technique will be successful.

Murman and Cole suggest an implicit, second-order-accurate, backward difference scheme as an alternate to the first-order-accurate, backward difference scheme that was used in the supersonic flow region. They hinted in their paper (see ref. 1), and it has been verified since, that calculations employing this second-order-accurate, backward difference scheme sometimes diverge during the relaxation iteration. Because of this difficulty, nearly all velocity potential calculations have been made with schemes accurate only to the first-order.

More recently, Warming and Beam (see ref. 20; see also Martin's work, ref. 21) have extended Murman's fully conservative scheme to the Euler equations. Although they were primarily concerned with the Euler equations, Warming and Beam suggested (but did not test) a second-order-accurate, backward difference scheme for the transonic small-disturbance equation, including

a shock-point operator and a parabolic point. We note that Murman's, as well as Warming and Beam's, second-order backward difference scheme is both dissipative and dispersive compared to Richtmeyer's standard (non-dissipative) scheme (see figs. 4A and 4B). The important questions concerning these second-order schemes, especially in our finite-element context, are why is the second-order-accurate scheme of Murman so much less reliable than his first-order scheme and will the alternative proposal of Warming and Beam alleviate this problem?

We begin by considering the latter of these two questions. We incorporated the second-order-accurate scheme of Warming and Beam into our version of Murman's code and tested it. The results of a few numerical experiments quickly showed that it fared no better than Murman's second-order-accurate scheme; it failed to converge reliably. We believe that the reason for the failure of both of these second-order-accurate schemes is closely tied to the parabolic point and its function in stabilizing the finite-difference scheme. Consequently, before presenting the modifications required to make second-order-accurate schemes converge, we first review the purposes for using the parabolic point.

The parabolic point in a finite-difference scheme serves the following three purposes:

a. First, it excludes the possibility of expansion shocks. In other words, the parabolic point ensures that the fluid experiences, at most, a finite (and not an infinite) acceleration. This point can be seen easily from the transonic small-disturbance equation itself:

$$(K\phi_x - \tfrac{1}{2}\phi_x^2)_x + (\phi_y)_y = 0 \ . \tag{12}$$

At the sonic point, we have

$$K - \phi_x = 0 , \qquad\qquad\qquad (13)$$

which indicates that $\phi_{yy} = 0$ at the sonic point only if ϕ_{xx} is bounded.

b. The second purpose of the parabolic point is to ensure consistency in the flux conservation across the sonic line, where the switching operators are employed.

c. Third (and perhaps most importantly) the parabolic point guarantees that the discretized system matrix can be inverted (and, if possible, constrains it to remain positive definite). To explain this point, we consider node P_1 in figure 4C. At point P_1 the test of whether the node is to be treated as subsonic or supersonic is based on the sign of the coefficient $K-\phi_x$ which is evaluated by means of central differences. Since the point P_1 is (by definition) supersonic, a backward difference at P_1 creates an inconsistency in the matrix which is removed when the parabolic condition $\phi_{yy} = 0$ is applied.

All three of these conditions are satisfied in the first-order-accurate, backward difference scheme if a single parabolic point is introduced; however, the same is not true for second-order schemes. In particular, point P_2 (see figure 4C) again introduces an inconsistency into the matrix if a second-order-accurate, backward difference scheme is used there. At successive supersonic points downstream of point P_2 , the second-order-accurate, backward difference formula can be applied without difficulty. Consequently, our suggested remedy is to introduce not one, but two parabolic points at the sonic line when second-order schemes are used in the supersonic region.

Using two parabolic points, we have done numerical experiments in which second-order-accurate formulas were used in both the subsonic and supersonic regions. The results have shown that the second-order schemes do converge reliably (with about the same number of iterations as is required for first-order schemes) when the second parabolic point is added. In order to obtain a second-order system that is completely analogous to Murman's first-order scheme, we also consider the requirements of a shock-point operator in a second-order scheme.

The shock-point operator serves some analogous (though not completely identical) purposes in cases where the flow switches from supersonic to subsonic, as the parabolic point does when the flow goes from subsonic to supersonic. When decelerating through the sonic point (whether discontinuously, as across a shock, or continuously, as across a decelerating sonic line), we introduce the shock-point operator for the following purposes:

a.   The shock-point operator allows for a discontinuity in ϕ_x.

b.   The shock-point operator ensures a consistent flux conservation in the presence of switching operators.

c.   The shock-point operator guarantees that the discretized system matrix can be inverted (and that it is positive definite, if possible).

Note that, except for the first, these purposes are identical to those of the parabolic operator. Item (a) in the parabolic list ensures that (expansion) shocks cannot occur; item (a) in the shock-point list ensures that (compression) shocks can occur.

To introduce our shock point, we start by analyzing Murman's shock-point operator for the *first-order-accurate scheme*. Using the nomenclature in the sketch below,

18
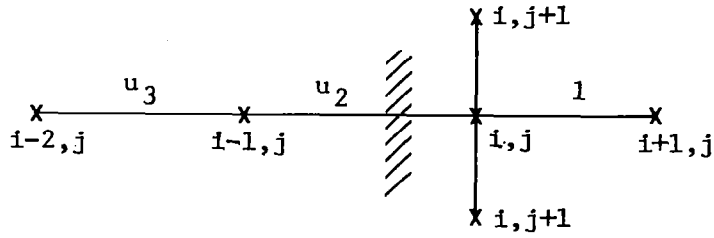
we have from equation (12)

$$(Ku_1 - \tfrac{1}{2}u_1^2) - (Ku_3 - \tfrac{1}{2}u_3^2) + \frac{\Delta x}{\Delta y^2} (\phi_{i,j+1} - 2\phi_{i,j} + \phi_{i,j-1}) = 0 \ . \quad (14)$$

Then, by adding and subtracting the quantity, $Ku_2 - \tfrac{1}{2}u_2^2$, Murman obtains

$$(Ku_1 - \tfrac{1}{2}u_1^2) - (Ku_2 - \tfrac{1}{2}u_2^2) + (Ku_2 - \tfrac{1}{2}u_2^2) - (Ku_3 - \tfrac{1}{2}u_3^2)$$

$$+ \frac{\Delta x}{\Delta y^2} (\phi_{i,j+1} - 2\phi_{i,j} + \phi_{i,j-1}) = 0 \ , \quad (15)$$

or

$$\left[K - \tfrac{1}{2}(u_1 + u_2)\right] (u_1 - u_2) + \left[K - \tfrac{1}{2}(u_2 + u_3)\right] (u_2 - u_3)$$

$$+ \frac{\Delta x}{\Delta y^2} (\phi_{i,j+1} - 2\phi_{i,j} + \phi_{i,j-1}) = 0 \ , \quad (16)$$

19

Murman then linearizes equation (16) by evaluating $(u_1 + u_2)/2$ and $(u_2 + u_3)/2$ using the most recent available values. Extensive numerical experiments have confirmed that the resulting scheme is stable and that the iteration converges with extremely good reliability.

The introduction of the shock-point operator for our second-order-accurate scheme must also be done with care. We begin by first considering a shock-point operator that is analogous to Murman's and then consider the one suggested by Warming and Beam (see ref. 20). Emphasis in both of these cases will be on satisfying all three of the purposes outlined above.

We use the notation in the sketch below.
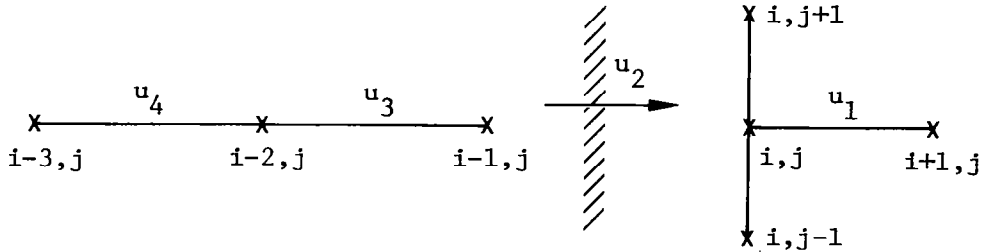
We allow a discontinuity in ϕ_x between points $i-1$ and i and obtain an elliptic shock-point operator with a derivative boundary condition for the velocity u_2 downstream of the shock. This boundary condition must be consistent with the locally normal shock-jump relation

$$u_2 = 2K - u_3 \quad ; \tag{17}$$

together, they give

$$\left[K - \left(\frac{u_1 + u_2}{2}\right)\right](u_1 - u_2) + \frac{\Delta x}{\Delta y^2}\left(\phi_{j+1} - 2\phi_j + \phi_{j-1}\right) = 0 . \tag{18}$$

Numerical experiments with this scheme have indicated that it allows reliable convergence in the relaxation iteration and that the results converge to the same limit reached with Murman's first-order-accurate scheme.

We have also obtained a second-order scheme that is formally equivalent to the one suggested by Warming and Beam. To obtain this scheme, we replace equation (17) by

$$u_2 = 2K - (2u_3 - u_4) \tag{19}$$

and substitute equation (19) into equation (18). Again, we obtain a stable scheme. Some results are given in figure 5. The effect of the shock-point operator is distinguishable in the fine grid calculations.

Use of an Elliptic Solver

In all numerical techniques for solving the transonic equation, some method of linearization is used to convert the nonlinear equation into a system of linear equations, which can then be solved by various means. The specific technique for linearizing the equation has a considerable effect on the amount of computer time that will be required to obtain the solution and may even determine whether the iteration for the nonlinearity converges or diverges. We now attempt to classify some methods for linearizing the equation, with emphasis on understanding how and why the Poisson technique works.

a. Picard (linearization by freezing coefficients)

$$(K - \phi_x^n)\phi_{xx}^{n+1} + \phi_{yy}^{n+1} = 0 \quad . \tag{20}$$

b. Rayleigh-Janzen (linearization about the equivalent incompressible flow)

$$K\phi_{xx}^{n+1} + \phi_{yy}^{n+1} = \phi_x^n \phi_{xx}^n \quad . \tag{21}$$

c. Newton-Raphson (Let $\phi^{n+1} = \phi^n + \delta\phi$, hence $J\delta\phi = -R(\phi^n)$ where J is the Jacobian and $R(\phi^n)$ is the residual. As a special case of this method, $J(\phi^n)$ is approximated by $\tilde{J}$ independent of n.)

$$\left[K - (\phi_x^n + \delta\phi_x)\right] (\phi_{xx}^n + \delta\phi_{xx}) + (\phi_{yy}^n + \delta\phi_{yy}) = 0 \quad , \tag{22}$$

which, neglecting second-order terms, gives

$$(K - \phi_x^n)\delta\phi_{xx} + \delta\phi_{yy} - \phi_{xx}^n\delta\phi_x = -R(\phi^n) \quad ,$$

where the right-hand side is the residual

$$R(\phi^n) = (K - \phi_x^n)\phi_{xx}^n + \phi_{yy}^n \quad . \tag{23}$$

Note that the Picard iteration is basically Murman's scheme (except the linearized coefficient is _updated_ during the iteration instead of after it), the Rayleigh-Janzen scheme is the one chosen by Martin (ref. 21) and is discussed at length below, while the Newton-Raphson scheme is similar to iterative schemes based on the unsteady small-disturbance equation.

22

In the Newton-Raphson scheme, the differential operator

$$(K - \phi_x^n) \frac{\partial^2}{\partial x^2} + \frac{\partial^2}{\partial y^2} - \phi_{xx}^n \frac{\partial}{\partial x} , \qquad (24)$$

which is the Jacobian of the small-disturbance equation, is of mixed type and switches character at the same location the original equation does. If we represent the Jacobian as

$$\alpha \frac{\partial^2}{\partial x^2} + \frac{\partial^2}{\partial y^2} + \frac{\beta}{\Delta x} \frac{\partial}{\partial x} , \qquad (25)$$

we note that it is very similar to the unsteady, small-disturbance equation,

$$(K - \phi_x)\phi_{xx} + \phi_{yy} - 2\phi_{xt} = 0 , \qquad (26)$$

where we associate ϕ_{xt} with $\phi_x^{n+1} - \phi_x^n$.

The convergence of these iterative methods for the case of elliptic equations has been studied extensively; however, their application to transonic flow represents an entirely different problem. Martin and Lomax (ref. 2) have suggested an iterative procedure for transonic flow, which is identical to the Rayleigh-Janzen technique. More specifically, they linearized the transonic

equation by placing the nonlinear term on the right-hand side and then solved the resulting Poisson equation by a direct matrix inversion (fast elliptic solver). After each iteration, the nonlinear right-hand side was updated. Their initial efforts were successful for transonic solutions that included very small supersonic regions; however, after applying special stabilizing procedures, they were able to extend the technique to free-stream Mach numbers, which allowed much larger supersonic bubbles. The obvious question that this technique raises is: How can a mixed-type equation be solved as a series of Poisson equations?

Jameson has reviewed this iterative approach and has shown that the technique fails for purely supersonic flows (see ref. 3); however, with the addition of an additional de-symmetrizing term to the Laplacian, the iteration can be made to converge, even in supersonic flow. Thus, we consider the solution of the equation

$$\alpha\delta\phi_{xx} + \frac{\beta}{\Delta x}\,\delta\phi_x + \delta\phi_{yy} = -R(\phi^n) \tag{27}$$

and use central differencing for $\delta\phi_{xx}$ and $\delta\phi_{yy}$ but use backward differencing for ϕ_x (and $R(\phi n)$) , to obtain

$$\alpha\partial_{xx}(\delta\phi) + \beta(\delta\phi_{i,j}^{n+1} - \delta\phi_{i-1,j}^{n+1})$$

$$+ \left(\frac{\Delta x}{\Delta y}\right)^2 \partial_{yy}(\delta\phi_{i,j}) = -\Delta x^2 R_{i,j}^n \ , \tag{28}$$

where $\partial_{xx}f = f_{i-1,j} - 2f_{i,j} + f_{i+1,j}$ and $\partial_{yy}f = f_{i,j-1} - 2f_{i,j} + f_{i,j+1}$.

For supersonic flows with periodic boundary conditions, the Von Neumann stability analysis shows that stability is obtained when $\beta > 2\alpha + |K\ell|$, where $K_\ell = K - \phi_x$. If β is chosen in this manner, we can use a fast direct solver to invert the left-hand side. Thus, we see that, if we attempt to solve the hyperbolic equation by a series of "elliptic" operators, we must add the (large) term $\beta\phi_x/\Delta x$ to ensure stability.

A heuristic analysis of this de-symmetrized operator shows that when $\beta/\Delta x$ is large enough to ensure stability, the operator is no longer elliptic. For example, consider the following difference scheme in the x direction:

$$(\Delta x^2)L_x = \alpha\partial_{xx}\delta\phi + \beta(\delta\phi_i - \delta\phi_{i-1})$$

$$= \alpha\delta\phi_{i+1} - 2\alpha\delta\phi_i + \alpha\delta\phi_{i-1} + \beta\delta\phi_i - \beta\delta\phi_{i-1} , \qquad (29)$$

which, after we regroup the terms, becomes

$$(\Delta x^2)L_x = (\alpha - \beta)\phi_{i-1} - (2\alpha - \beta)\phi_i + \alpha\phi_{i+1} . \qquad (30)$$

Defining the new parameter

$$\alpha' = (2\alpha - \beta)/2 , \qquad (31)$$

we can rewrite equation (30) as

$$(\Delta x^2)L_x = \left(\alpha' - \frac{\beta}{2}\right)\phi_{i-1} - 2\alpha'\phi_i + \left(\alpha' + \frac{\beta}{2}\right)\phi_{i+1} , \qquad (32)$$

which is a valid approximation for

$$L_x = \alpha' \left[\phi_{xx} + O(\Delta x^2) \right] + \frac{\beta}{\Delta x} \left[\phi_x + O(\Delta x^2) \right]. \tag{33}$$

It is immediately obvious that the type of equation (33) depends upon the sign of α' , which can, in turn, be controlled by the magnitude of β . Thus, if $\beta > 2\alpha$, the equation becomes hyperbolic, and we see that the Von Neumann criterion for stability in supersonic regions is equivalent to requiring that the left-hand side operator be made hyperbolic.

If we now return to equation (27) and use central differencing for ϕ_x , we see (by again following our heuristic argument) that it is not possible to change the type of the equation. Similarly, the Von Neumann condition also indicates that the Poisson iteration for the wave equation will not converge when central differencing is used for the $\partial/\partial x$ term. Thus, we see that it is not this term alone, but rather the unsymmetrical differencing of it, that allows convergence. The introduction of the asymmetric term ϕ_x in backward-difference form is necessary for convergence because it removes the elliptic nature of the left-hand side operator and causes it to be hyperbolic.

We have conducted a numerical experiment based on this idea by using a line-relaxation version of the analysis of Martin and Lomax. Instead of using the primitive variables u and v , we use the velocity potential ϕ . The line relaxation should effectively introduce the precise term ϕ_{xt} (or $\delta\phi_x$) , which is needed for convergence. The solution does indeed converge and the results are shown in figure 6.

The special stabilization procedure referred to above, which Martin and Lomax used, was a u_t term. The use of this de-symmetrizing term allowed them

to extend the technique to transonic flows with large supersonic bubbles. As we noted above, we argue that this de-symmetrization term is effective because it changes the type of the left-hand side operator in the supersonic region so that it is no longer elliptic.

FINITE ELEMENTS

Hyperbolic Methods

Finite-element procedures can be applied directly to hyperbolic schemes; in particular, the Lax-Wendroff scheme applied directly over the finite-element formulation (finite element in space, finite difference in time). Thus, if we consider a Taylor series expansion in time, we have

$$u(t + \Delta t) = u(t) + \dot{u}\Delta t + \tfrac{1}{2}\ddot{u}\Delta t^2 , \tag{34}$$

and if

$$\frac{\partial u}{\partial t} = \frac{\partial F(u)}{\partial x} , \tag{35}$$

we can express

$$\ddot{u} = \frac{\partial}{\partial x} \left(A \frac{\partial F}{\partial x} \right) , \tag{36}$$

where A is the Jacobian of F(u) ,

$$A_{ij} = \frac{\partial F_i}{\partial u_j} \quad . \tag{37}$$

Hence,

$$u(t + \Delta t) = u(t) + \frac{\partial F}{\partial x} \Delta t + \frac{\Delta t^2}{2} \frac{\partial}{\partial x} \left(A \frac{\partial F}{\partial x} \right) \quad . \tag{38}$$

Examples of using finite-element procedures to solve Lax-Wendroff schemes such as these have been given by Oden (ref. 22), who used a Galerkin procedure.

If an explicit artificial viscosity term is added, we obtain an equation that is similar to the one studied by Wahlbin (ref. 23). When the explicit artificial viscosity term is added, the transonic equation, in its small-disturbance form, becomes

$$u_t = K_\ell u_x + v_y + \varepsilon u_{xx} \quad , \tag{39}$$

$$v_t = u_y - v_x \quad . \tag{40}$$

If we now represent the velocity in terms of a shape function ψ as

$$u = \psi_i(x,y) \; U_i(t) \tag{41}$$

$$v = \psi_i(x,y) \; V_i(t) \tag{42}$$

and apply a Galerkin procedure, equations (39) and (40) become

$$\iint \left(\psi_i \, U_{i,t} \, \psi_j \right) \, dx \, dy = \iint \left(K_\ell \, \psi_{i,x} \, U_i \, \psi_j \right) \, dx \, dy$$

$$+ \iint \left(\psi_{i,y} \, V_i \, \psi_j \right) \, dx \, dy + \iint \left(\varepsilon \, \psi_{i,xx} \, U_i \, \psi_j \right) \, dx \, dy \qquad (43)$$

and

$$\iint \left(\psi_i \, V_{i,t} \, \psi_j \right) \, dx \, dy = \iint \left(\psi_{i,y} \, U_i \, \psi_j \right) \, dx \, dy - \iint \left(\psi_{i,x} \, V_i \, \psi_j \right) \, dx \, dy \, .$$

$$(44)$$

These can be written in the more compact form

$$M_{ij} \, \frac{dU_i}{dt} = K_\ell K_{ji} U_i + C_{ji} V_i + \varepsilon d_{ij} U_i \qquad (45)$$

$$M_{ij} \, \frac{dV_i}{dt} = C_{ji} U_i - K_{ji} V_i \qquad (46)$$

by defining the matrices

$$M_{ij} = \iint \psi_i \psi_j \, dx \, dy \, , \qquad (47)$$

29

$$K_{ji} = \iint \frac{\partial \psi_i}{\partial x} \psi_j \, dx \, dy \ , \tag{48}$$

$$C_{ji} = \iint \frac{\partial \psi_i}{\partial y} \psi_j \, dx \, dy \ , \tag{49}$$

$$D_{ji} = \iint \frac{\partial \psi_i}{\partial x} \frac{\partial \psi_j}{\partial x} \, dx \, dy \ . \tag{50}$$

For the special case of linear shape functions and rectangular elements, the functions ψ_i become

$$\psi_1 = \left(1 - \frac{x}{h_1}\right)\left(1 - \frac{y}{h_2}\right) \qquad \psi_2 = \frac{x}{h_1}\left(1 - \frac{y}{h_2}\right)$$

$$\psi_3 = \frac{x}{h_1}\frac{y}{h_2} \qquad\qquad \psi_4 = \left(1 - \frac{x}{h_1}\right)\frac{y}{h_2} \tag{51}$$

so that the matrices C, D, K, and M become

$$C_{ji} = \frac{h_1}{12}
\begin{bmatrix}
-2 & -1 & 1 & 1 \\
-1 & -2 & 2 & 1 \\
-1 & -2 & 2 & 1 \\
-2 & -1 & 1 & 2
\end{bmatrix} \tag{52}$$

$$D_{ji} = \frac{h_2}{6h_1} \begin{bmatrix} 2 & -2 & -1 & 1 \\ -2 & 2 & 1 & -1 \\ -1 & 1 & 2 & -2 \\ 1 & -1 & -2 & 2 \end{bmatrix} \tag{53}$$

$$K_{ji} = \frac{h_2}{12} \begin{bmatrix} -2 & 2 & 1 & -1 \\ -2 & 2 & 1 & -1 \\ -1 & 1 & 2 & -2 \\ -1 & 1 & 2 & -2 \end{bmatrix} \tag{54}$$

and

$$M_{ji} = \frac{h_1 h_2}{36} \begin{bmatrix} 4 & 2 & 1 & 2 \\ 2 & 4 & 2 & 1 \\ 1 & 2 & 4 & 2 \\ 2 & 1 & 2 & 4 \end{bmatrix} \tag{55}$$

Implicit schemes are recommended for solving either these systems or ordinary differential equations in time so that stability restrictions can be avoided, especially in the latter case where the ϕ_{tt} term appears.

Kreiss and Scherer have reviewed the convergence of iterative schemes such as these (see ref. 24) and have shown that they are always stable for semi-bounded operators. Swartz and Wendroff have reached similar conclusions for Burger's equation (see ref. 25). The disadvantage of using techniques of this type is that the mass matrix must be inverted at each step. This effect can, however, be diminished by going to the lumped mass formulation.

In passing, we mention that, instead of the Galerkin method, the least-squares method may be used (in space) in the same way Carasso solved the wave equations (ref. 26) and a coupled system of wave and heat equations (ref. 27).

We also mention an interesting work by Mote (ref 28). Mote has considered the use of global-local finite elements, where the known characteristics of the global solution to the problem of interest are exploited. For example, the global behavior of the incompressible flow solution could be used in a global-local scheme for transonic flow. Note, in addition, that some global methods (in the classical sense of Ritz) have been applied to compressible and even transonic flow as early as twenty years ago by Wang (ref. 29). His computations did not include any shocks, although he suggested a shock-fitting procedure.

Finally, we should note the important parallel between transonic flow and shallow-water theory. The hydraulic analogy leads to equations of motion that are identical to the transonic equations if the ratio of specific heat γ is taken to be 2.0. A comparison between finite-difference and finite-element techniques for shallow-water theory has been given by Weare (ref. 30). We note without comment that he concluded finite-difference procedures were more economical for this problem (see also ref. 31).

<div align="center">Mixed-Type Methods</div>

<div align="center">Introductory Remarks – Some Simplified Models for the Transonic
Small-Disturbance Equations</div>

According to the transonic small-disturbance approximation, the stream-lines are almost parallel to the x axis, and the nonlinear effects occur only in the x terms, as can be seen directly from the following small-disturbance equation:

$$(K - \phi_x)\phi_{xx} + \phi_{yy} = 0 \ . \tag{56}$$

A one-dimensional version of this equation,

$$(K\phi_x - \tfrac{1}{2}\phi_x^2)_x = 0 \, , \tag{57}$$

has been studied by Bauer et al. (ref. 32). By treating P as a general matrix and ϕ as a vector, we can extend Bauer's equation to the more versatile form

$$(K\phi_x - \tfrac{1}{2}\phi_x^2)_x + P\phi = 0 \, , \tag{58}$$

which corresponds to not one, but a system of, ordinary differential equations. This latter system, equation (58), is almost identical to the transonic equation, and it can be obtained from the transonic equation by a step that we shall refer to as semi-discretization. By semi-discretization, we mean that ϕ is continuous in x , but is discrete in y . As an example, we can use central differencing to approximate ϕ_{yy} in equation (56) and so can arrive immediately at equation (58), where the matrix P is given by

$$P = \frac{1}{\Delta y^2} \begin{bmatrix} -2 & 1 & & & \\ 1 & -2 & 1 & & \\ & \ddots & \ddots & \ddots & \\ & & 1 & -2 & 1 \\ & & & 2 & -2 \end{bmatrix} \tag{59}$$

To complete the system, we must modify the first and last rows of P by applying the boundary conditions.* Similar representations can also be obtained by applying the Method of Moments or by applying a finite-element technique in space (in the y direction only).

After some appropriate discretization in y has been applied to the transonic equation, the resulting equation (58) can be categorized for either subsonic flow or supersonic flow by the following two classical systems of equations:

   a.   The case of subsonic flow is closely analogous to the two-point boundary value problem

$$- (Q\phi_x)_x + P\phi = 0 \ , \tag{60}$$

which is the one-dimensional, steady-state heat equation.

   b.   The case of supersonic flow is closely analogous to the initial heat value problem

$$- (M\dot{\phi})^{\cdot} + P\phi = 0 \ , \tag{61}$$

which is the equation for a mass-spring system.

A separate body of literature exists for each of these equations; transonic flow represents a combination of both of them. In the subsonic region, the equation is elliptic (boundary-value in nature), while in the supersonic

---

*Note that P can be diagonalized: A system of uncoupled ODE's can be constructed if the eigenvalues and eigenvectors of the matrix are known.

34

region it is hyperbolic (initial-value in nature). The nonlinearity of the transonic equation is essential since this nonlinearity is responsible for the transition from one region to the other. The nonlinearity also permits compression and expansion shock waves to occur (i.e., a discontinuous transition from hyperbolic to elliptic).

The application of finite-element techniques to the two-point BVP corresponding to equation (60) is well established. Applications of finite-element procedures to initial value problems, like equation (61), have also been used in the field of structural dynamics; however, usually finite-difference methods are used for this equation. Thus, the general pattern is that finite-element procedures are used more often than finite-difference procedures for boundary-value problems, but that finite-difference techniques are used more frequently for initial-value problems. In the present transonic case, the question of which technique to use is not as obvious since the transonic equation is of mixed-type and encompasses both types of equations.

A Comparison of Various Discretization Techniques

In this section we compare three distinct methods that can be used to discretize a partial differential equation. These three methods are finite differences, finite volumes, and finite elements.

Discretization methods. - The construction of a finite-difference scheme is usually based on a Taylor series expansion. The stability of the resulting difference scheme can then be easily investigated in a linear, local sense by applying the Von Neumann stability analysis, as long as the grid system is rectangular. Heuristic stability analyses, which again rely on a Taylor series, can also be useful in categorizing the truncation error as either dissipative

or dispersive. Boundary conditions are easily included in a finite-difference scheme when the boundaries are rectangular, but when the boundaries become nonrectangular or irregular, their finite-difference representations become cumbersome and inaccurate. Thus, the application of boundary conditions or irregular boundaries represents one of the key weaknesses of finite-difference procedures.

In the finite-volume technique, the principal idea is to convert the differential equation into its integral form before applying discretization procedures. The advantage of this approach is that it transforms the differential equations, which are really mathematical expressions of certain conservation laws, into a form that allows the conservation of these same quantities to be verified and enforced easily in the discrete system.

The third type of discretization, finite elements, can be obtained by applying either a variational principle (such as the one used in classical mechanics) or a weighted residual method. The weighted residual methods, in turn, include Galerkin techniques and least-squares methods. Finite-volume techniques can be considered as specific realizations of the method of weighted residuals (the method of subdomains).

Applications of discretization techniques to elliptic problems. - The classical five-point formula for the Laplace equation represents an interesting example of the application of the three techniques described above (see Varga's discussion). For the case considered here, the same five-point formula can be derived by means of a Taylor series expansion (finite difference), by conservation of flux across imaginary boundaries (finite volume), or by means of finite-element techniques based on triangular elements and linear shape functions

as shown for the first time by Courant.* Although all these techniques lead to

identical results for the Laplace equation on a uniform grid system, in general,

they lead to different schemes.

As an example of the types of differences that are generated when the

three techniques are applied in more general circumstances, we again consider

the Laplace operator; but this time, instead of considering the five-point

formula, we consider the nine-point scheme in the sketch below,
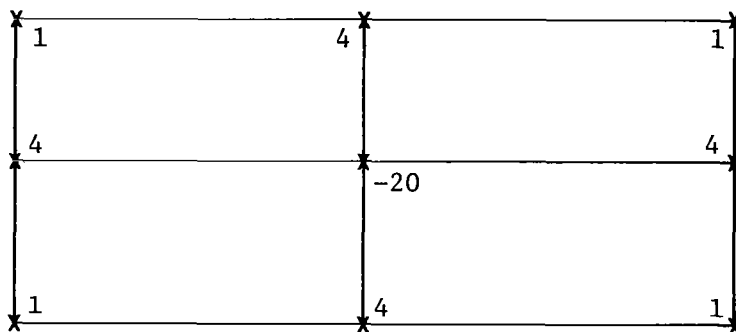
which can be expressed as the linear combination of the following two five-

point formulae.

Four

Plus One

Finite-volume techniques, which are based on replacing the area integral by an equivalent line integral (Gauss's theorem) in the following fashion,
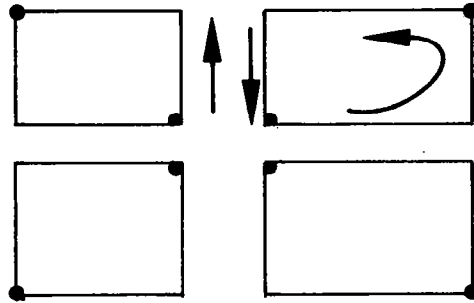
give a result which is equivalent to the finite-difference representation
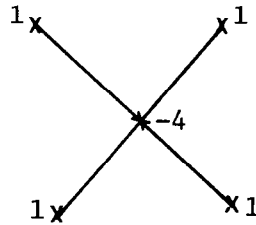
if linear shape functions are used on rectangular elements, with a weighting function, which is unity, inside the domain and zero outside. Note that because of the cancellation on the interior sides of the line integration, only the corner points appear in the finite-volume representation.

Finally, the use of finite-element techniques based on a variational principle, result in a discretization that can be expressed as
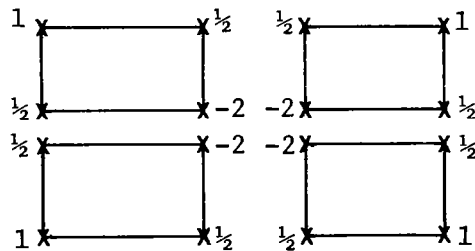
and that, in finite-difference terms, is equivalent to the equally weighted sum of the finite-difference formulae
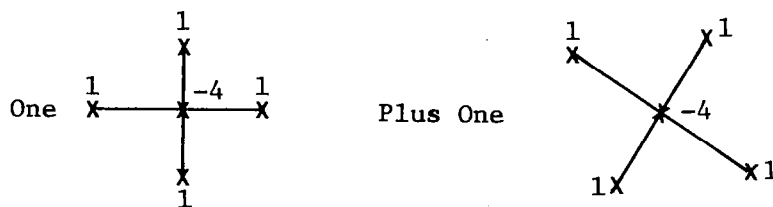
Birkhoff and Gulati have considered general discretization procedures for linear source problems, with a view towards determining optimal, few-point representations (see ref. 33). Their comparative study considers both five-point and nine-point discretizations on regular mesh, along with some discussion of the three-point analogs for the corresponding one-dimensional case. The results show that global accuracy of five-point formulae could never be greater than $O(h)$ when the grid was nonuniform, nor better than $O(h^2)$ when the grid was uniform, regardless of how the formulae were obtained. This accuracy is, of course, exactly the accuracy that is cbtained with standard five-point, finite-difference formulae. They also demonstrated that the optimal accuracy for the nine-point formula was $O(h^4)$ with a uniform rectangular mesh and that it deteriorated to $O(h^2)$ for a nonuniform mesh. This order of accuracy is equivalent to that achieved by the Rayleigh-Ritz method, with bilinear approximating functions.

As an example of the use of higher-order elements, we consider the application of piecewise-continuous cubics to the discretization step. The dependent variables can be represented by cubics through the use of three distinct elements (shown in the sketch below): (1) cubics for which cnly the function itself is constrained to be continuous at the nodes (e.g., serendipity

elements); (2) Hermite cubics for which the function and its (two) first derivatives are continuous at the nodes; and (3) cubic splines (tensor product of a one-dimensional spline) whose second-derivatives are continuous at the nodes.
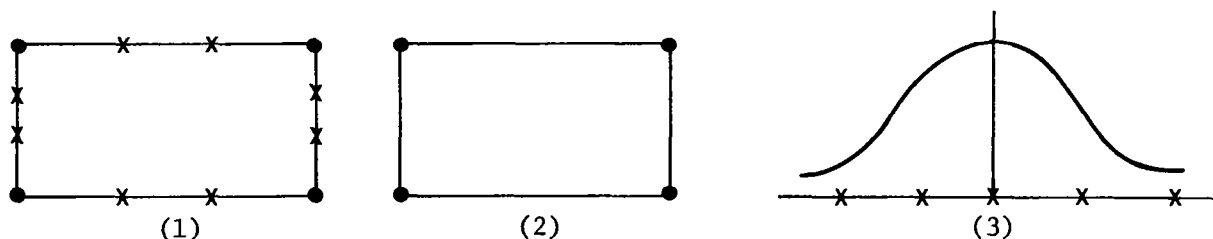
Since cubic splines require more grid points and are restricted to rectangular elements, we actually compare only the Lagrange and Hermite cubics. The Hermite cubic formulation seems to be more accurate. Later, we give some numerical results for incompressible flow over a parabolic-arc airfoil to demonstrate this accuracy. For the sake of comparison, we also discuss a mixed variational principle that uses linear shape functions in ϕ , $u(=\phi_x)$ and $v(=\phi_y)$. As noted previously, such lower-order elements can be used in conjunction with extrapolation techniques (such as Richardson's) to obtain higher-order accuracy.

Wheeler (ref. 34) has analyzed another method of obtaining very accurate approximations of the flux values at particular points in the domain for the two-point boundary value problem. This method is based on evaluating the moment of a Galerkin solution of the problem, and it reduces the error in the flux from $O(h^r)$ to $O(h^{2r})$. Such improvements in the computation of the flux appear quite attractive for a velocity potential solution for which the flux is the principal quantity of interest.

<u>Applications of discretization techniques to hyperbolic problems</u>. - For the
wave equation, the literature can be divided into two categories, namely, those
algorithms that use finite-element techniques in space but finite differences in
time, and those algorithms that use finite elements in both space and time. It
is interesting to note that most of the work concerned with developing mathemat-
ically rigorous proofs of the characteristics of the discretized system have
used a combination of finite-element and finite-difference techniques, while
most of the work using only finite elements has been more engineering oriented.

Examples of work in the first category include the efforts of Birkhoff
and Dougalis (ref. 35), Swartz and Wendroff (ref. 25), Swartz (ref. 36),
Vichnevetsky and De Schutter (ref. 37), Vichnevetsky and Pfeiffer (ref. 38),
and Goudrea and Taylor (ref. 39). On the basis of their work on the wave equa-
tion, Birkhoff and Dougalis recommend the Numerov scheme, which is a combination
of both finite differences and finite elements in space. The Numerov scheme
takes advantage of the fact that the phase errors in finite-element and finite-
difference schemes are opposite in sign, and by the use of a proper combination
of the two phase errors, obtains a scheme with excellent dispersive properties.

Goudrea and Taylor evaluated different numerical integration methods in
structural dynamics, including the methods of Newmark, Wilson, and Houboult.
Argyris et al. (ref. 40) have generalized the Newmark family of schemes and
they were able to obtain unconditionally stable schemes by incorporating
a few simple modifications.

Finite-element techniques in space and time have been studied by Argyris
(see refs. 40 and 41), Fried (ref. 42), and Zienkiewicz and Lewis (ref. 43).
The work of Argyris and Fried is based on Hamilton's principle. In their
work, they do not allow the function at the end point to vary (as is tradition-
ally done in a Hamiltonian approach), but they do allow the magnitude of the

41

initial velocity to vary. This method is similar to the method of inverse shooting, which was used in our previous paper (ref. 44). In that work we also replaced the initial value problem by an equivalent boundary value problem.

Zienkiewicz and Lewis have based their work on Galerkin or least-squares techniques. They use Hermite cubics and consider both the end position and the velocity as unknowns; thus, they obtain a series of weighted residual equations.

Some algebraic examples of finite-element formulae for initial value and boundary value problems. - To illustrate the differences between these various discretization techniques, we consider a simple, one-dimensional example problem:

$$\phi_{xx} - \phi = 0 . \tag{62}$$

We have constructed formulae for both elliptic (boundary value) and hyperbolic (initial value) problems (using Hermite cubics as shape functions) for each of three finite-element procedures, namely, the Hamiltonian, the Galerkin, and the least-squares techniques. The results are summarized in figures 7 and 8, where we present the influence coefficients corresponding to equation (62) for the node between two adjacent (one-dimensional) elements.

As an example, we describe the procedure for determining the Galerkin results in detail so that the diagrams in figures 7 through 9 can be more clearly understood.

We define the numerical representation of ϕ in equation (62) over any element in terms of the Hermite interpolating polynomials $\beta_i(x)$, as

$$\Phi = \beta_i(x)\chi_i , \quad i = 1,4 , \tag{63}$$

where the parameters χ_i represent the unknowns (the influence coefficients) determined for each element. The Hermite polynomials are cubic curves that are defined over each element and that satisfy the following four sets of boundary conditions at the ends of the interval $(0,h)$. (Since the polynomials are cubic, we can specify four end conditions in each interval.)

Function / Boundary Condition	$\beta_i(0)$	$\beta_i'(0)$	$\beta_i(h)$	$\beta_i'(h)$
$\beta_1(x)$	1	0	0	0
$\beta_2(x)$	0	0	1	0
$\beta_3(x)$	0	1	0	0
$\beta_4(x)$	0	0	0	1

Thus, each polynomial satisfies one unity boundary condition and three homogeneous conditions. Algebraically, these polynomials are defined as

$$\beta_1(x) = 1 - 3(x/h)^2 + 2(x/h)^3 \ , \tag{64}$$

$$\beta_2(x) = 3(x/h)^2 - 2(x/h)^3 \ , \tag{65}$$

$$\beta_3(x) = \left[x/h - 2(x/h)^2 + (x/h)^3 \right] h \ , \tag{66}$$

$$\beta_4(x) = \left[-(x/h)^2 + (x/h)^3 \right] h \ . \tag{67}$$

By the usual Galerkin procedure, we choose a weighting function ψ and require that the equations, after being multiplied by ψ, be satisfied on the

43

average over the interval (0,h) corresponding to one element. Thus, we require

$$\int_0^h (\Phi_{xx}\psi - \Phi\psi) \, dx = 0 \qquad (68)$$

and immediately integrate by parts to give

$$\int_0^h (\Phi_x\psi_x + \Phi\psi) dx = \text{B.T.} \, , \qquad (69)$$

where B.T. refers to boundary terms occurring at the ends of the element. We now choose the weighting function ψ to be equal to the polynomial β_i corresponding to the appropriate degree of freedom. Then, using the numbering system defined below for a single element,

$$
\begin{array}{ccc}
\Phi & 1 & 2 \\
\Phi_x & 3 & 4
\end{array}
$$
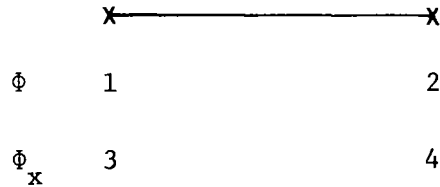
we compute the influence coefficients, in turn, for the function and its derivative at the right end and, then, at the left end.

The influence coefficients for the function ϕ_2 at the right end of the element are given by

$$\int_0^h (\Phi_x \psi_x + \Phi\psi)dx = \int_0^h \left\{ (\beta_1' \beta_2' + \beta_1 \beta_2)\chi_1 \right.$$

$$+ (\beta_2'^2 + \beta_2^2)\chi_2 + (\beta_3' \beta_2' + \beta_3 \beta_2)\chi_3$$

$$\left. + (\beta_4' \beta_2' + \beta_4 \beta_2)\chi_4 \right\} dx = \text{B.T.} \,, \tag{70}$$

where the weighting function for point 2 is β_2. After performing the indicated integration, we obtain the following relation between the four values of χ_i,

$$\left(\frac{54h}{420} - \frac{36}{30} \right)\chi_1 + \left(\frac{156h}{420} + \frac{36}{30} \right)\chi_2 +$$

$$\left(\frac{13h^2}{420} - \frac{1}{10} \right)\chi_3 + \left(-\frac{22h^2}{420} - \frac{1}{10} \right)\chi_4 = \text{B.T.} \tag{71}$$

If we repeat this integration for the degree of freedom number four (ϕx at the right end) here, using β_4 as the weighting function, we obtain a similar relation, and similarly, for the two degrees of freedom at the left-hand end. The results are summarized in figure 7.

Having derived the influence coefficients for each degree of freedom in terms of the other degrees of freedom in the same element, we now combine two elements and obtain the appropriate influence coefficient for the center point in terms of the six (total) degrees of freedom in the two elements. Defining two elements A and B and using the following notation,

45

$$
\begin{array}{c}
\text{A} \qquad\qquad \text{B} \\
\text{X}\!\!-\!\!\!-\!\!\!-\!\!\!-\!\!\!-\!\!\!-\!\!\!-\!\!\text{X}\!\!-\!\!\!-\!\!\!-\!\!\!-\!\!\!-\!\!\!-\!\!\!-\!\!\text{X}
\end{array}
$$

ϕ	1	2	3
ϕ_x	4	5	6
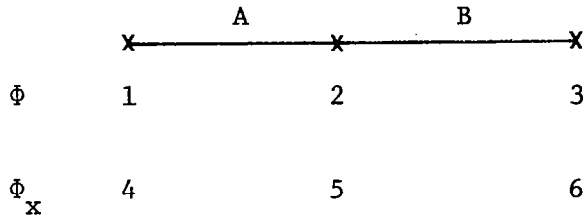
we obtain, for the second degree of freedom (for the value of ϕ at the center), which is the left end of element B and the right end of element A:

$$
\left(\frac{54h}{420} - \frac{36}{30}\right)\chi_1 + \left(\frac{156h}{420} + \frac{36}{30}\right)\chi_2 + \left(\frac{13h^2}{420} - \frac{1}{10}\right)\chi_4
$$

$$
+ \left(-\frac{22h^2}{420} - \frac{3}{30}\right)\chi_5 + \left(\frac{156h}{420} + \frac{36}{30}\right)\chi_2 +
$$

$$
\left(\frac{54h}{420} - \frac{36}{30}\right)\chi_3 + \left(\frac{22h^2}{420} + \frac{3}{30}\right)\chi_5 + \left(-\frac{13h^2}{420} + \frac{1}{10}\right)\chi_6 = 0 , \tag{72}
$$

which is an equation for χ_2 in terms of χ_1, χ_3, χ_4, χ_5, and χ_6. A similar application gives a second equation for degree of freedom number five, which corresponds to the derivative ϕ_x at the intersection between the two elements. The influence coefficients for ϕ are summarized in figure 8A, along with similar results that have been obtained with the least-squares procedure. The results obtained from the Hamiltonian method are identical to those for the Galerkin procedure and have not been rewritten in figure 8A. Figure 8B gives the same comparison of influence coefficients, but this time for ϕ_x .

The supersonic (initial value) case can also be computed from the results shown in figure 7; but, when the two elements are considered together, the downstream element must not have any effect on the solution for the influence coefficients corresponding to the central point. Again, using the

notation from the sketch on the previous page, we write the relationship for χ_2 in the supersonic case as

$$\left(\frac{54h}{420} - \frac{36}{30}\right)\chi_1 + \left(\frac{156h}{420} + \frac{36}{30}\right)\chi_2 +$$

$$\left(\frac{13h^2}{420} - \frac{3}{30}\right)\chi_4 + \left(-\frac{22h^2}{420} - \frac{3}{30}\right)\chi_5 = \text{B.T.} \quad . \tag{73}$$

These Galerkin results for the supersonic problem are summarized in figure 9 in a format identical to that used for the subsonic case (figure 8). Again, Hamiltonian and least-squares results are also shown. Note that in the initial value case the Hamiltonian results (where the method of inverse shooting has been used) differ from the Galerkin results. Also note that the downstream points do not contribute to the solution at the central point.

Influence coefficients for a two-dimensional example. - Similar tables for a two-dimensional case (partial differential equation) are given in figures 10 through 12. For this case, we have considered the Laplacian equation:

$$\phi_{xx} + \phi_{yy} = 0 \tag{74}$$

for the elliptic case, and the wave equation,

$$-\phi_{xx} + \phi_{yy} = 0 \tag{75}$$

for the hyperbolic case. Again, these tables are based on the Hermitian interpolating polynomials.

Chan and Brashears (ref. 45) have applied a least-squares procedure to transonic flows. In this work, the upstream effects are zeroed out in the supersonic region. This procedure is identical with the one proposed by Zienkiewicz and Lewis for the wave equation (see ref. 43).

Schemes for Transonic Flow

In a previous paper, Hafez, Murman, and Wellford (ref. 44) derived two distinct finite-element schemes for the transonic small-disturbance equation. These two schemes used different discretization criteria for their development. The first scheme uses a finite-element technique in the space-like variable (y) and a finite-difference representation in the time-like variable (x). The only difference between this finite-element scheme and Murman's scheme is in the mass matrix. If a lumped mass is used, the scheme reduces identically to Murman's; if a consistent (Graham) matrix is used, the schemes remain distinct. In the consistent-mass matrix formulation, three y levels of the x equations are coupled. Comparison with Murman's results show that the two calculations are almost identical (differences occur only in the fourth decimal place); i.e., the lumped-mass (finite-difference) and the consistent-mass (finite element in space) methods give comparable results.

The second scheme described by Hafez, Murman, and Wellford is the "inverse shooting" technique, which uses a finite-element discretization in both the space-like and the time-like variables. Unlike the first scheme, the inverse shooting scheme is not unconditionally stable. We can show this readily by writing the scheme in the form of Von Neumann and Lees:

$$K_\ell \phi_{xx_{C.D.}} = \phi_{yy_{C.D.}} + h^2 \omega \phi_{xxyy}; \quad K_\ell = \left| K - \phi_x \right|, \tag{76}$$

48

where the subscript C.D. refers to central difference (see ref. 46). Von Neumann and Lees showed that this equation was unconditionally stable only when $\omega \leq \frac{1}{2}$. The corresponding value for ω in our scheme is $\omega = (K\ell + 1)/6$. By analogy to the system of Von Neumann and Lees, we see that our system is non-dissipative and that it has dispersive properties that depend on ω.

Because of the conditional stability of equation (76), it is evident that terms proportional to ϕ_{xxyy} and ϕ_{yyx} (a dissipative term) are needed. In particular, if these terms are added with the proper multiplicative coefficient, the scheme becomes identical to the backward-difference scheme used by Murman. If linear shape functions and rectangular elements are used, the finite-element representation of both ϕ_{xxyy} and ϕ_{yyx} becomes identical to their counterparts obtained from centered finite differences. When higher-order shape functions are used for the finite-element representation, it no longer remains obvious that these two terms sufficiently guarantee stability. Fortunately, however, Showalter (ref. 47) has obtained a rigorous answer to this question. He studied two nonstandard methods for integrating the initial value problem

$$B\ddot{\phi} + A\phi = f \tag{77}$$

in a Hilbert space using Galerkin projection techniques. The first method, when applied to the equation

$$\frac{\partial^2 \phi}{\partial t^2} - \Delta\phi = f \tag{78}$$

(where Δ refers to the Laplacian), is

$$\frac{\partial^2 \phi}{\partial t^2} - \varepsilon\Delta \frac{\partial \phi}{\partial t} - \Delta\phi = f(x,t) \ , \tag{79}$$
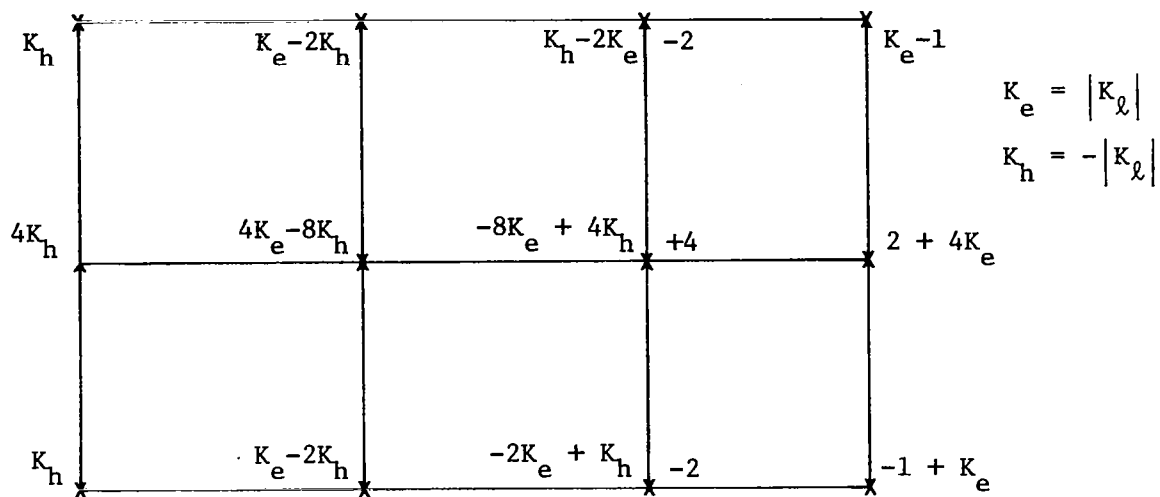
where ε is restricted to be positive. The second method, applied to the same equation, has the form

$$\frac{\partial^2 \phi}{\partial t^2} - \varepsilon\Delta \frac{\partial^2 \phi}{\partial t^2} - \Delta\phi = f(x,t) \ . \tag{80}$$

In this model, these regularizations represent artificial viscosity or artificial inertia. In our simple example, Δ is replaced by $\partial^2/\partial y^2$ so that the first term is ϕ_{yyt} and the second term is ϕ_{yytt}. Some numerical examples, using artificial viscosity and artificial inertia, that have been obtained from our finite-element model are shown in figures 13 and 14. Again, we have used line-relaxation methods to obtain these solutions.

As discussed in our previous work, the introduction of blending elements is crucial to the success of a transonic-flow computational technique. For example, if we use a centered finite-difference approximation of ϕ_{yy} in the sonic element rather than a Galerkin approximation, the calculation sometimes diverges, and, even when it does converge, more iterations are required. Some examples of this behavior are given in figure 15.

The second blending element used in these calculations is a finite-element, shock-point operator, whose specific form is shown in the sketch below.

K_h $K_e - 2K_h$ $K_h - 2K_e$ -2 $K_e - 1$

$4K_h$ $4K_e - 8K_h$ $-8K_e + 4K_h$ $+4$ $2 + 4K_e$

K_h $K_e - 2K_h$ $-2K_e + K_h$ -2 $-1 + K_e$

$$K_e = |K_\ell|$$
$$K_h = -|K_\ell|$$

The same results can be obtained with locally normal shock-fitting, namely

u_{j+1}

u_j

u_{j-1}
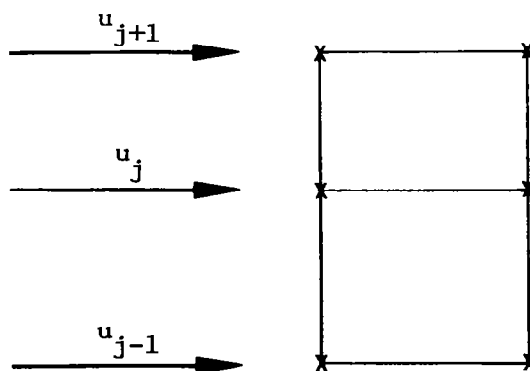
where u_j , u_{j+1} , u_{j-1} are velocities that satisfy the normal shock polar relation. These results are shown in figures 13 and 14.

51

Elliptic Methods

A Mixed Variational Principle for Transonic Flow

When developing finite-element approximation methods, we might benefit from a variational development of the appropriate differential equations. In this variational development, we introduce functionals whose Euler equations are equivalent to equation (1). Initially, we introduce the "primal functional" $J(\phi)$ where ϕ is the perturbation velocity potential. This functional is given as follows:

$$J(\phi) = \frac{1}{2} \int_\Omega (K_1 \phi_x^2 + \phi_y^2)dx\,dy$$

$$- \frac{1}{6} \int_\Omega K_2(\phi_x)^3 dx\,dy\;, \tag{81}$$

where $K_1 = 1 - M_\infty^2$, $K_2 = M_\infty^2(1 + \gamma)$. For the moment we disregard the boundary conditions. For simplicity, we consider the Dirichlet boundary conditions (ϕ is specified on all boundaries). The first variation of the functional $J(\phi)$ is defined for arbitrary η satisfying the boundary conditions by

$$\delta J(\phi) = \underset{\varepsilon \to 0}{\text{LIM}}\ \frac{J(\phi + \varepsilon\eta) - J(\phi)}{\varepsilon}\;. \tag{82}$$

The second variation $\delta^2 J(\phi)$ of the functional $J(\phi)$ is defined similarly. By setting the first variation of the functional equal to zero and applying the fundamental theorem of the calculus of variations, we get the following result:

Theorem 1: The Euler equation corresponding to $J(\phi)$ is

52

$$(K_1 - K_2 \phi_x)\phi_{xx} + \phi_{yy} = 0 \ . \tag{83}$$

Taking the second variation of $J(\phi)$, we get

Theorem 2: For arbitrary η satisfying the boundary conditions

$$\delta^2 J(\phi) = \int_\Omega \left[(K_1 - K_2 \phi_x)\eta_x^2 + \eta_y^2 \right] dx \ dy \tag{84}$$

From equation (84) we determine a basic property of the variational method. For subsonic flow, $\delta^2 J(\phi) \geq 0$ because $K_1 - K_2\phi_x > 0$. But, for strongly super-critical (transonic) flow, $K_1 - K_2\phi_x < 0$ for many points in Ω . Thus, the second variation of the functional $J(\phi)$ has no definite sign for the case of transonic flow. A method for iteratively approximating this problem (essentially, the variational analog of the standard procedure of shifting the nonlinear term to the right-hand side of the equation), however, is to find the critical points of a new functional $\overline{J}(\phi(n+1))$, which is defined as follows:

$$\overline{J}(\phi^{(n+1)}) = \frac{1}{2} \int_\Omega \left(K_1 {\phi_x^{(n+1)}}^2 + {\phi_y^{(n+1)}}^2 \right) dx \ dy$$

$$- \frac{1}{2} \int_\Omega K_2 {\phi_x^{(n)}}^2 \phi_x^{(n+1)} \ dx \ dy \ . \tag{85}$$

The Euler equation of this functional is

$$K_1 \phi_{xx}^{(n+1)} + \phi_{yy}^{(n+1)} = K_2 \phi_x^{(n)} \phi_{xx}^{(n)} \ . \tag{86}$$

53

The second variation of $\bar{J}(\phi^{(n+1)})$ is

$$\delta^2 \bar{J}(\phi^{(n+1)}) = \int_\Omega (K_1 \eta_x^2 + \eta_y^2) \, dx \, dy \; . \tag{87}$$

Since $K_1 > 0$, we get

$$\delta^2 \bar{J}(\phi^{(n+1)}) \geq 0 \quad , \text{ for all n .} \tag{88}$$

Thus, in the iterative scheme, the second variation $\delta^2 \bar{J}$ is always positive, while in the original problem the second variation $\delta^2 J$ is indefinite. This inconsistency serves as a mathematical (rather than physical) explanation of the nonconvergence of iteration equation (86) to supercritical flow solutions observed by Martin and Lomax (ref. 2) and Chan and Brashears (ref. 45). The discrepancy noted above is the motivation for the approach developed in this paper.

A mixed formulation can be developed by letting ϕ be the perturbation velocity potential and by letting u be the x component of the perturbation velocity. Then, a mixed function $I(\phi,u)$ associated with the small-disturbance transonic problem is given as follows:

$$I(\phi,u) = \frac{1}{2} \int_\Omega (K_1 \phi_x^2 + \phi_y^2) dx \, dy$$

$$- \frac{1}{2} \int_\Omega K_2 u^2 \phi_x \, dx \, dy + \frac{1}{3} \int_\Omega K_2 u^3 \, dx \, dy \quad . \tag{89}$$

We define the first variation of I with respect to ϕ and u by $\delta_\phi I$ and $\delta_u I$. By setting $\delta_\phi I = 0$ and $\delta_u I = 0$, we obtain the following result.

54

Theorem 3: The Euler equations corresponding to the functional $I(\phi,u)$ are

$$K_1\phi_{xx} - K_2uu_x + \phi_{yy} = 0 \tag{90a}$$

$$u - \phi_x = 0 \tag{90b}$$

The second variations of I with respect to ϕ and u are denoted by $\delta_\phi^2 I$ and $\delta_u^2 I$, respectively. From equation (89) we obtain the following.

Theorem 4: The second variations of the functional $I(\phi,u)$ relative to the parameters ϕ and u are

$$\delta_\phi^2 I = \int_\Omega (K_1\eta_x^2 + \eta_y^2)dx\ dy\ , \tag{91a}$$

$$\delta_u^2 I = \int_\Omega K_2\phi_x\eta^2\ dx\ dy\ , \tag{91b}$$

where η is a variation in ϕ or u.

Clearly, the second variations behave as shown below:

$$\delta_\phi^2 I \geq 0\ ,$$

$$\delta_u^2 I > 0 \qquad \phi_x \text{ positive },$$

$$\delta_u^2 I < 0 \qquad \phi_x \text{ negative }.$$

The present formulation thus allows us to divide the domain of the flow Ω into regions (usually two in number) in which the sign of the second variation of the function with respect to ϕ and u is always known. In contrast, if we use the primal formulation for transonic flow, the sign of the second variation is indefinite so it is not possible to specify specific regions in which the second variation has a specific sign. Suppose we let Ω_1 be the part of the domain Ω in which ϕ_x is positive and Ω_2 be the part of the domain Ω in which ϕ_x is negative. Then $\Omega = \Omega_1 \cup \Omega_2$. We let $I_1(\phi,u)$ be the functional I restricted to Ω_1. We let $I_2(\phi,u)$ be the functional I restricted to Ω_2. Then, the solution to problem (1) can be characterized as the set (ϕ^*,u^*) such that

$$\underset{u}{\text{MIN}} \ \underset{\phi}{\text{MIN}} \ I_1(\phi,u) = I_1(\phi^*,u^*) \tag{92a}$$

$$\underset{u}{\text{MAX}} \ \underset{\phi}{\text{MIN}} \ I_2(\phi,u) = I_2(\phi^*,u^*) \ . \tag{92b}$$

In Theorem 3, we have verified that the correct differential equations [corresponding to equation (1)] result from the mixed variational principle. We now rewrite the functional to include the proper boundary terms. In approximation procedures, the set of boundary conditions for the infinite domain Ω is normally replaced by the following set on a finite domain (also called Ω):

$$(1 + \phi_x) \frac{dg}{dx} - \phi_y = 0 \ , \ \text{on the airfoil} \tag{93a}$$

$$\phi_y = 0 \ , \ \text{on} \ y = 0 \ \text{upstream and downstream of the airfoil} \tag{93b}$$

$$\phi = \text{far-field solution} \quad .$$ (93c)

For simplicity, we neglect ϕ_x relative to 1 in equation (93a). The resulting boundary condition is

$$\phi_y = \frac{dg}{dx} \quad , \text{ on a slit } \partial\Omega_b \quad .$$ (94)

This boundary condition can also be handled iteratively as in Chan and Brashears (ref. 45). We included this iterative application of the boundary condition in our analysis, but we do not discuss it here. Then, we let $d\tilde{s}$ be the arc length along $\partial\Omega_b$ in x,y space. We now introduce a mixed functional $\bar{I}(\phi,u)$, which includes the natural Neumann boundary condition along $\partial\Omega_b$:

$$\bar{I}(\phi,u) = \frac{1}{2} \int_\Omega (K_1\phi_x^2 + \phi_y^2)\, dx\ dy$$

$$- \frac{1}{2} \int_\Omega K_2 u^2 \phi_x\ dx\ dy + \frac{1}{3} \int_\Omega K_2 u^3\ dx\ dy$$

$$- \int_{\partial\Omega_b} \frac{dg}{dx} \phi(\tilde{s})\ d\tilde{s} \quad .$$ (95)

Taking the first variation of $\bar{I}(\phi,u)$ with respect to ϕ , we obtain, as Euler equations, equation (90a) and

$$\phi_{\tilde{n}} = \frac{dg}{dx} \quad .$$ (96)

Since the functional $\overline{I}(\phi,u)$ is developed for the small-disturbance formulation (which assumes a very thin body) to within the order of the approximation used, $\phi_{\underset{\sim}{n}} \simeq \phi_y$. Thus, the boundary condition [equation (94)] is satisfied. When varying $\overline{I}(\phi,u)$, we obtain one additional integral associated with $\partial\Omega_1$. This term occurs when we integrate the second term on the right in equation (95) by parts in x , and we obtain an integral over dy (the thickness of the airfoil). Since in small-disturbance theory we assume the thickness of the airfoil is small, we can assume this term is negligible. In fact, in most finite-difference approximations, the boundary conditions are applied not on the body, but on the chord. Then, the integral in question disappears.

A Mixed Finite-Element Model For Transonic Flow

To develop a finite-element model for transonic flow, we divide the domain Ω into finite elements Ω_e . Then,

$$\Omega = \bigcup_{e=1}^{E} \Omega_e \ ,$$

where E is the total number of elements in the domain. On each domain Ω_e we introduce an approximation for the potential function ϕ and the perturbed x velocity component u of the following form:

$$\Phi_e(x,y) = \Psi_i(x,y)\Phi_i \ , \tag{97a}$$

$$U_e(x,y) = \beta_i(x,y)U_i \ , \tag{97b}$$

where $\Psi_i(x,y)$ and $\beta_i(x,y)$ are finite-element interpolation (shape) functions, and ϕ and U are values of the potential function ϕ and the velocity u at the nodes of the element.

The index notation (involving i) in equation (97a) and (97b) implies that a summation should be performed over the number of nodes in the element. In terms of (Φ_e, U_e), the functional $\overline{I}$ takes the following form:

$$\overline{I}(\Phi_e, U_e) = \frac{1}{2} K_{ij} \Phi_i \Phi_j - \frac{1}{2} L_{ijk} U_i U_j \Phi_k$$

$$+ \frac{1}{3} M_{ijk} U_i U_j U_k$$

$$- F_j \Phi_j \, , \tag{98}$$

where

$$K_{ij} = \int_{\Omega_e} (K_1 \Psi_{i_x} \Psi_{j_x} + \Psi_{i_y} \Psi_{j_y}) \, dx \, dy \, ,$$

$$L_{ijk} = \int_{\Omega_e} K_2 \beta_i \beta_j \Psi_{k_x} \, dx \, dy \, ,$$

$$M_{ijk} = \int_{\Omega_e} K_2 \beta_i \beta_j \beta_k \, dx \, dy \, ,$$

$$F_j = \int_{\partial\Omega_1} \frac{dg}{dx} \Psi_j \, d\tilde{s} \, .$$

59

The finite-element analog of the variational procedure [equation (92)] is to require that the functional $\overline{I}(\Phi_e, U_e)$ have a stationary value relative to variations in Φ_j and U_i. We set

$$\frac{\partial \overline{I}(\Phi_e, U_e)}{\partial \Phi_j} = 0 \,,$$

(99a)

$$\frac{\partial \overline{I}(\Phi_e, U_e)}{\partial U_i} = 0 \,.$$

(99b)

From equation (98) in conjunction with equation (99),

$$K_{ij} \Phi_i = \frac{1}{2} L_{ikj} U_i U_k + F_j$$

(100a)

$$\frac{\partial \overline{I}}{\partial U_i} = -L_{ijk} U_j \Phi_k + M_{ijk} U_j U_k$$

(100b)

$$= 0 \,.$$

Equations (100a) and (100b) represent the finite-element equilibrium equations for a single element Ω_e. The corresponding equations for the entire domain Ω are obtained with standard assembly techniques (see ref. 22).

Dual Iterative Solution Algorithms

The use of a combination of direct solution and gradient algorithms to solve the algebraic equations obtained from mixed-finite element models was initially proposed by Ciarlet and Glowinski in conjunction with the biharmonic

60

equation (unpublished data from P. Ciarlet and R. Glowinski, 1975). These methods have become known as "dual iterative methods." We adopt the same approach here. The variational problem [equation (92)] involves a minimization procedure in ϕ and a minimization-maximization procedure (in different domains) in U. We solve for the ϕ variable, using a direct solution method, since $\delta^2_\phi I$ is always positive, and we solve for the U variable, using a gradient method, which locally accounts for the sign change of $\delta^2_U I$. We thus introduce the following direct-gradient algorithm for the small-disturbance transonic flow calculation (for ρ = constant > 0):

$$K_{ij} \, \phi_i^{(n+1)} = \frac{1}{2} L_{ikj} \, U_i^{(n)} U_k^{(n)} + F_j \, , \qquad (101a)$$

$$U_j^{(n+1)} = U_j^{(n)} + C \, \rho \, \frac{\partial \overline{I}^{(n)}}{\partial U_j} \, , \qquad (101b)$$

where

$$\frac{\partial \overline{I}^{(n)}}{\partial U_j} = -L_{jik} \, U_i^{(n)} \, \phi_k^{(n+1)} + M_{jik} \, U_i^{(n)} U_k^{(n)}$$
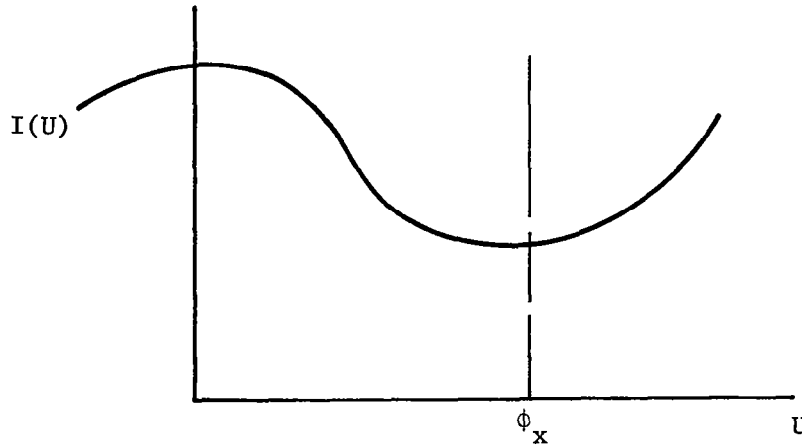
and

$$C = 1 \qquad\qquad \delta^2_{U_j} \, \overline{I}^{(n)} \leq 0 \, ,$$

$$C = -1 \qquad\qquad \delta^2_{U_j} \, \overline{I}^{(n)} > 0 \, ,$$

where

61

$$\delta_{U_j}^2 \overline{I}^{(n)} = \frac{\partial^2 \overline{I}^{(n)}}{\partial U_j^2} = -L_{jjk} \phi_k^{(n+1)} + 2M_{jjk} U_k^{(n)} \qquad (102)$$

for each element. From (100b) we see that the gradient of $\overline{I}$ relative to U_i is zero if $U_j = 0$ for all nodes in the element. In fact, we see that the variation of $\overline{I}$ with U for positive ϕ_y varies, as shown in the sketch below.

To prevent convergence of the algorithm to the trivial solution $U = \phi_x = 0$, we choose C as shown in the chart below:

ϕ_x Positive		
$\delta_U I$	$\delta_U^2 I$	C
negative	negative	-1
negative	positive	-1
positive	positive	-1
positive	negative	1

62

ϕ_x Negative		
$\delta_U I$	$\delta_U^2 I$	C
negative	positive	1
negative	negative	1
positive	negative	1
positive	positive	-1

We treat the gradient solution step as the integration of a time-dependent equation in the incremental time parameter t

$$\frac{\partial U_j^{(n)}}{\partial t} = c \frac{\rho}{\Delta t} \frac{\partial \overline{I}^{(n)}}{\partial U_j} , \tag{103}$$

where Δt is the increment of incremental time t , or

$$\frac{\partial U_j^{(n)}}{\partial t} = f(U_k^{(n)}) .$$

Numerical experiments have shown two deficiencies in the iterative algorithm. First, for transonic flow, there is no convergence to shock-wave solutions. Second, the iterative scheme seems to oscillate about the solutions.

Artificial Viscosity Models

To obtain the correct generalized solution for the transonic flow problem, we introduce artificial viscosity. Let ε_1 be a positive constant. The gradient algorithm augmented by artificial viscosity is

$$U_t = \frac{C\rho}{\Delta t} U(U-\phi_x) - \frac{\rho \varepsilon_1}{\Delta t} U_x \; .$$

(104)

We use equation (104) in regions where ϕ_x is positive $(C = -1)$. Differentiating equation (104), with respect to x, introducing the result in equation (90a), and assuming $U \approx \phi_x$, we obtain the following equation:

$$K_1 \phi_{xx} + \phi_{yy} = K_2 \phi_x \phi_{xx} - \frac{K_2 \varepsilon_1}{2} \phi_{xxx} - \frac{K_2 \Delta t}{2\rho} \phi_{xxt} \; .$$

(105)

If we assume that the iteration converges, the last term on the right goes to zero, and the resulting equation is

$$K_1 \phi_{xx} + \phi_{yy} = K_2 \phi_x \phi_{xx} - \frac{K_2 \varepsilon_1}{2} \phi_{xxx} \; ,$$

(106)

where ϕ_{xxx} is the artificial viscosity term. This term damps the ϕ equation. To provide convergence in the U equation, we introduce another viscosity term into equation (104). For a positive constant ε_1 (used only when $\phi_x > 0$), we get

$$U_t = \frac{C\rho}{\Delta t} U(U-\phi_x) - \frac{\rho\varepsilon_1}{\Delta t} U_x + \frac{\rho\varepsilon_2}{\Delta t} U_{xx} \quad . \tag{107}$$

The last term on the right introduces a viscous term into the U equation. Introducing a finite-element analog for the last two terms on the right-hand side in equation (104) and incorporating these into equation (101b), we obtain the following expression:

$$U_j^{(n+1)} = U_h^{(n)} + C\rho \frac{\partial \bar{I}^{(n)}}{\partial U_j} - \frac{\rho\varepsilon_1}{\Delta t} D_{ij} U_i^{(n)}$$

$$- \frac{\rho\varepsilon_2}{\Delta t} E_{ij} U_i^{(n)} \quad , \tag{108}$$

where

$$D_{ij} = \int_{\Omega_e} \beta_{ix}\beta_j \ dx \ dy \qquad E_{ij} = \int_{\Omega_e} \beta_{ix}\beta_{jx} \ dx \ dy \ .$$

We developed a computer program DUALIT to solve the equations formulated above. This code contains all of the features of the subsonic programs, SUBSON1 and SUBSON2, described in the Appendix.

Numerical Results

We did test calculations for flow about a 6-percent parabolic-arc airfoil with the mesh of eight-node serendipity elements shown in figure 16. For these calculations, $\varepsilon_1 = 1.4 \times 10^{-2}$ and $\varepsilon_2 = 0.7 \times 10^{-3}$. In figure 17

we compare the resulting C_p distribution to the results of Murman for $K = 1.8$ ($M_\infty = 0.875$) .

A GENERAL SHOCK-FITTING PROCEDURE FOR FINITE ELEMENTS

A more general shock-fitting procedure, which was previously used by Wellford and Oden in elastodynamics (see ref. 48), can be applied to transonic flows. We demonstrate this application by starting from the unsteady transonic small-disturbance equation from Cheng and Hafez (ref. 14):

$$\alpha\phi_{xt} = (K - \phi_x)\phi_{xx} + \phi_{yy} \ . \tag{109}$$

We obtained this equation directly from the unsteady velocity potential equation by ignoring the "high frequency" term (ϕ_{tt}) , and we can also use it to represent the iterative (relaxation) procedure (except perhaps with a different value of α). We proceed with development of our general shock-fitting procedure by obtaining the weak solution of this time-dependent equation, which will enable us to predict the shock's movement (both its displacement and its speed).

We represent the shock shape by the function

$$f(x,y,t) = 0 \ , \tag{110}$$

which we assume can be inverted to give the x position of the shock

$$x - x^D(y,t) = 0 \ . \tag{111}$$

66

Using this nomenclature, we write the jump conditions admitted by the weak solution of the unsteady equation as

$$[\![\alpha f_t \phi_x - f_x(K\phi_x - \tfrac{1}{2}\phi_x^2) \; f_y\phi_y]\!] = 0 \; , \tag{112}$$

where $[\![\;]\!]$ represents the jump across the discontinuity. With equation (111), we can rewrite equation (112) as

$$\alpha \frac{\partial x^D}{\partial t} \; [\![\phi_x]\!] \; + \; [\![K\phi_x - \tfrac{1}{2}\phi_x^2]\!] \; - \frac{\partial x^D}{\partial y} \; [\![\phi_y]\!] \; = 0 \; , \tag{113}$$

and defining the speed of the shock as $S = \partial x/\partial t$, we have

$$[\![\phi_x]\!] \; S\alpha \; = \; - \; [\![K\phi_x - \tfrac{1}{2}\phi_x^2]\!] \; + \frac{\partial x^D}{\partial y} \; [\![\phi_y]\!] \; . \tag{114}$$

The corresponding jump condition admitted by weak solution for the irrotationality condition

$$\phi_{xy} = \phi_{yx} \tag{115}$$

is

$$[\![f_x\phi_y - f_y\phi_x]\!] \; = 0 \tag{116}$$

or

$$[\![\phi_y]\!] \; + \frac{\partial x^D}{\partial y} \; [\![\phi_x]\!] \; = 0 \; . \tag{117}$$

Combining equations (114) and (117) gives

$$[\![\phi_x]\!] \, S\alpha = - \, [\![K\phi_x - \tfrac{1}{2}\phi_x^2]\!] \left(\frac{\partial x^D}{\partial y}\right)^2 [\![\phi_x]\!] \tag{118}$$

or, in its final form, the equation for the speed of the shock is

$$S = \frac{\partial x}{\partial t} = -\tfrac{1}{2}\left\{ \langle K - \phi_x \rangle \, [\![\phi_x]\!] + \left(\frac{dx^D}{dy}\right)^2 \right\}. \tag{119}$$

If the flow field approaches a steady state, the shock speed vanishes so that in the steady state, equation (119) reduces to

$$\langle K - \phi_x \rangle \, [\![\phi_x]\!] + \left(\frac{\partial x}{\partial y}\right)^2 = 0 \, , \tag{120}$$

which is of course the jump relation obtained from the steady-state equations.

The strength of the unsteady shock $[\![\phi_x]\!]$ can be evaluated from the Hadamard kinematical compatibility equation

$$\frac{d \, [\![F]\!]_S}{dt} = \left[\!\left[\frac{\partial F}{\partial t}\right]\!\right]_S + U_S \left[\!\left[\frac{\partial F}{\partial x}\right]\!\right]_S + V_S \left[\!\left[\frac{\partial F}{\partial y}\right]\!\right]_S \, , \tag{121}$$

where the subscript S refers to the shock. For our case, $F = \phi_x$, hence,

68

$$\frac{d\,[\![\phi_x]\!]_S}{dt} = \left[\!\!\left[\frac{\partial^2\phi}{\partial x\partial t}\right]\!\!\right]_S + U_S \left[\!\!\left[\frac{\partial^2\phi}{\partial x^2}\right]\!\!\right]_S + V_S \left[\!\!\left[\frac{\partial^2\phi}{\partial x\partial y}\right]\!\!\right]_S \; , \qquad (122)$$

where

$$U_S = \frac{dx^D}{dt} \;, \quad V_S = \frac{dy^D}{dt} \; . \qquad (123)$$

The shock jump relation can be incorporated into a finite-element procedure by applying finite differences in time to equation (119) in a manner analogous to that of Wellford and Oden:

$$X^{n+1} - X^n = -\beta \left\{ <K - \phi_x> \; [\![\phi_x]\!] + \left(\frac{\partial x}{\partial y}\right)^2 \right\}^n \; , \qquad (124)$$

where $\beta = \Delta t/\alpha$. (Note that we can use a similar formula for relaxation procedures, except that now β corresponds to a relaxation factor.) A similar finite-difference procedure can be used in conjunction with equation (122) to update $[\![\phi_x]\!]$. As in most numerical procedures, an explicit technique of the type suggested in equation (124) imposes a maximum allowable step size because of stability considerations.

As a passing remark, we note that when the transition from subsonic to supersonic (or from supersonic to subsonic) is smooth, the present finite-element algorithm is consistent since we automatically require that $\phi_{yy} = 0$.

A similar shock-fitting procedure can also be applied to the full potential equation:

$$\rho_t = -(\rho U)_x - (\rho v)_y \; , \qquad (125)$$

where, because of the irrotationality assumption, we can express the density ρ as a function of the velocity only as follows:

$$\rho = \rho(u,v) \ .$$ (126)

Defining the velocity potential ϕ as

$$u = \phi_x \ , \quad v = \phi_y$$ (127)

so that

$$\phi_{xy} = \phi_{yx}$$

$$\phi_{xt} = \phi_{tx}$$

$$\phi_{yt} = \phi_{ty} \ ,$$

we can write the expression for the weak solution of equation (125) as

$$[\![\rho f_t + \rho u f_x + \rho v f_y]\!] = 0 \ ,$$ (128)

where

$$f_t : f_x : f_y = [\![\phi_t]\!] \quad : \quad [\![\phi_x]\!] \quad : \quad [\![\phi_y]\!] \ .$$

Then, following the development of the small-perturbation equation, we arrive at an analogous expression for the shock velocity and strength. Although this procedure appears quite promising, it has not yet been tested in either a finite-difference or a finite-element formulation.

EXTENSIONS TO THE FULL POTENTIAL EQUATION

Although the full velocity potential equation is algebraically more complicated than the small-disturbance equation, the crucial factor that makes the full potential equation more difficult to solve is that the direction of the velocity vector in the full potential case is not known. Jameson (ref. 3) has developed some type-dependent finite-difference schemes and some relaxation techniques that work well for the full potential equation, but the corresponding finite-element analog is not obvious.

Hyperbolic Methods

One exception to this difficulty is when the equation is formulated in its complete unsteady form. In this case, the equation is always hyperbolic, and, as a result, the use of type-dependent differencing (which relies on a knowledge of the orientation of the local velocity vector) is not required. Consequently, finite-element techniques (in space) can be applied in a straightforward manner. This capability for bypassing type-dependent differencing and retaining central differences throughout the flow-field is not limited to the unsteady Euler formulation; other hyperbolic schemes can also be used.

As a first example, we consider the fully hyperbolic scheme

$$u_t = (\rho u)_x + (\rho v)_y \tag{129a}$$

71

$$v_t = u_y - v_x \ .$$

<div align="right">(129b)</div>

Magnus and Yoshihara (ref. 12), using a finite-difference technique, solved this formulation numerically, but abandoned it because relaxation methods (velocity potential) were much faster. They used the Lax-Wendroff finite-difference scheme, with a special mesh arrangement near the airfoil leading edge.

The weak solution consistent with equations (129a) and (129b) is

$$[\![u]\!] \ f_t - [\![\rho u]\!] \ f_x - [\![\rho v]\!] \ f_y = 0 \ .$$

<div align="right">(130)</div>

Note that this weak solution is different from the one discussed in the proceeding section where the continuity equation

$$\rho_t + (\rho u)_x + (\rho v)_y = 0$$

<div align="right">(125)</div>

was used. Also, note that the flow field described by equations (129a) and (129b) becomes irrotational only in the limit of a steady solution.

As indicated above, finite-element procedures can be applied directly to hyperbolic schemes such as these. In particular, we can take the Lax-Wendroff scheme directly to a finite-element formulation (finite element in space, finite difference, or iterative, in time) and thereby introduce the artificial viscosity that is necessary for the convergence of the hyperbolic formulation.

72

Elliptic Methods

We begin by considering the full potential equation

$$\left(1 - \frac{u^2}{a^2}\right)\phi_{xx} - \frac{2uv}{a^2}\phi_{xy} + \left(1 - \frac{v^2}{a^2}\right)\phi_{yy} = 0 \qquad (132a)$$

or

$$(\rho\phi_x)_x + (\rho\phi_y)_y = 0 \qquad (132b)$$

and identify three classical schemes that can be used to linearize the equation as follows:

a.   Picard method (linearization by freezing coefficients),

$$\left(1 - \frac{u^{n^2}}{a^{n^2}}\right)\phi_{xx}^{n+1} - \frac{2u^n v^n}{a^{n^2}}\phi_{xy}^{n+1} + \left(1 - \frac{v^{n^2}}{a^{n^2}}\right)\phi_{yy}^{n+1} = 0 \qquad (133a)$$

or

$$\left(\rho^n \phi_x^{n+1}\right)_x + \left(\rho^n \phi_y^{n+1}\right)_y = 0 \qquad (133b)$$

b.   Rayleigh-Janzen method (linearization about the equivalent incompressible flow),

$$\phi_{xx}^{n+1} + \phi_{yy}^{n+1} = -\left(-\frac{u^{n^2}}{a^{n^2}}\phi_{xx}^n - \frac{2u^n v^n}{a^{n^2}}\phi_{xy}^n - \frac{v^{n^2}}{a^{n^2}}\phi_{yy}^n \right) \tag{134a}$$

or

$$\phi_{xx}^{n+1} + \phi_{yy}^{n+1} = -\frac{1}{\rho^n}\left(\rho_x^n \phi_x^n + \rho_y^n \phi_y^n \right) \tag{134b}$$

c.   Newton-Raphson method,

Let $\quad \phi^{n+1} = \phi^n + \delta\phi$ $\hspace{4cm}$ (135)

and $\quad J\delta\phi = -R(\phi^n)$ $\hspace{4cm}$ (136a)

or $\quad J\phi^{n+1} = J\phi^n - R(\phi^n)$ $\hspace{4cm}$ (136b)

where J is the Jacobian and $R(\phi^n)$ is the residual.

The Rayleigh-Janzen scheme is the one used by Jameson (ref. 3) and it converges only for subsonic flows. For transonic flows, Jameson uses a *two-step iterative procedure*, in which a fast solver is followed by a line relaxation procedure. The first step can be calculated by finite elements. Although there is no analogy for the second step, we discuss some related work below.

Application of Optimal Control Methods to Transonic Flow

Following Glowinski and Pironneau (ref. 49), we consider the minimization problem,

$$\int \left\{ (\phi_x - u)^2 + (\phi_y - v)^2 \right\} dx \, dy \tag{137}$$

with the constraints

$$(\phi_{xx} + \phi_{yy}) = - \left\{ (K - u)u_x + v_y \right\} + u_x + v_y \, . \tag{138}$$

Wellford and Hafez (ref. 50) used a similar procedure based on a mixed variational principle, which allowed special treatment of the supersonic region. Thus, instead of constructing a functional whose Euler equation include the irrotationality condition and applying the continuity equation as a constraint [as in equations (137) and (138)], they constructed a functional whose Euler equations included both the irrotationality condition and the continuity condition. This functional can be written in terms of ϕ and u as

$$I(\phi,u) = \iint \left[\frac{1}{2}(K\phi_x^2 + \phi_y^2) - \frac{1}{2} u^2 \phi_x + \frac{1}{3} u^3 \right] dx \, dy \, . \tag{139}$$

Then, again using the gradient method, we obtain the alternative scheme,

$$\delta\phi = -\omega \left[K\phi_{xx} + \phi_{yy} - uu_x \right], \tag{140a}$$

$$\delta u = -\omega' u(u - \phi_x) + \varepsilon_1 u_x + \varepsilon_2 u_{xx} \, . \tag{140b}$$

75

In their work, Wellford and Hafez require $\omega'u$ to be positive by choosing ω' negative when u is negative, while choosing ω to be very large, so that equation (140a) becomes

$$K\phi_{xx} + \phi_{yy} = uu_x .$$ (141)

Note that the term $\varepsilon_2 u_{xx}$ is necessary to prevent the iteration from diverging. The artificial viscosity term will ensure proper behavior, including the compression shock (and excluding the expansion shock), in the supersonic region.

These two methods can also be applied to the full potential equation. Glowinski and Pironneau minimize the functional

$$\int \left[(u - \phi_x)^2 + (v - \phi_y)^2 \right] dx \, dy$$ (142)

with the constraint

$$\phi_{xx} + \phi_{yy} = \omega \left\{ (\rho u)_x + (\rho u)_y \right\} + u_x + v_y$$ (143)

and

$$\rho = \left[1 + \frac{\gamma-1}{2} (u^2 + v^2) \right]^{\frac{1}{\gamma-1}} .$$ (144)

The functional in equation (142) can also be solved by a mixed variational principle in terms of ϕ , u , and v , by a direct extension of Wellford and Hafez's work. Performing the required extension leads to

76

$$I(\phi, u, v) = \iint \frac{\lambda}{2} \left[(\phi_x - u)^2 + (\phi_y - v)^2 \right]$$

$$+ \rho \left[(u^2 - u\phi_x) + (v^2 - v\phi_y) \right] - C\rho^\gamma , \qquad (145)$$

where

$$C = 1/\gamma M_\infty^2 \qquad (146)$$

The minimization of equation (145) yields the following three expressions:

From $\partial I/\partial \phi = 0$, we have

$$\lambda(\phi_{xx} + \phi_{yy}) = \left[(\rho u)_x + (\rho v)_y \right] + \lambda \left[u_x + v_y \right] \quad ; \qquad (147a)$$

from $\partial I/\partial u = 0$, we obtain

$$\lambda(u - \phi_x) = \rho(\phi_x - u) + \rho_u(u\phi_x - u^2) + \rho_v(v\phi_y - v^2) \quad ; \qquad (147b)$$

and, from $\partial I/\partial v = 0$, we obtain

$$\lambda(v - \phi_y) = \rho(\phi_y - v) + \rho u(u\phi_x - u^2) + \rho v(v\phi_y - v^2) , \qquad (147c)$$

where λ is a free parameter.

Additional regularization terms like those introduced for the TSDE are needed for the convergence of iterations based on this scheme; however, in this scheme, regularization terms are needed for both the u and the v equations.

77

One approach is to use, in the supersonic region, artificial viscosity terms analogous to those used by Jameson in his finite-difference formulation.

For the subsonic region, the elliptic equation may be put into the Poisson form and solved iteratively as before. Again, convergence is guaranteed for the elliptic region; hence, in the subsonic region, I_u and I_v can be replaced by the simpler relations $u = \phi_x$ and $v = \phi_y$ to save computer storage space.

SUMMARY AND CONCLUSIONS

We have presented a review of finite-element and finite-difference techniques for transonic flow calculations. For the transonic small-disturbance equation with linearized boundary conditions, Murman's finite-difference scheme is preferred over finite-element procedures, especially if some of the more recent acceleration procedures (e.g., multi-grids) are used. Such a comparison with finite elements is based on rectangular elements with linear shape functions. If higher-order shape functions or mixed formulations with fewer elements are used, and if a rapid, direct inversion technique is used, the finite-element method becomes more attractive. Treatment of the nonlinear mixed equation must include the transition from one region to another, and to allow only for a compression shock; the technique must have some provision for excluding expansion shocks.

Hopefully, finite-element methods will retain their advantages in the treatment of boundary conditions for the full potential equation. An unsteady (hyperbolic) approach for applying finite-element procedures to the full potential equation has been outlined. Without efficient methods for accelerating the iterative procedure, however, this method will not be economical.

Finally, we have looked for optimal control methods for transonic flow; but, without the inclusion of artificial viscosity or shock-fitting procedures, we do not expect the calculation of transonic flow fields with large supersonic regions to be successful.

Flow Research Company

21414-68th Avenue South

Kent, Washington 98031

June 14, 1978

APPENDIX

FINITE-ELEMENT SOLUTIONS USING GAUSSIAN ELIMINATION

(FRONTAL SOLVER)

As part of this research, we developed two codes to calculate subsonic flows using standard finite-element techniques. Both programs solve incompressible and small-distrubance flows about arbitrary bodies, and both could be easily extended to a full potential formulation.

The first program (SUBSON1) uses two-dimensional isoparametric elements of the serendipity type.
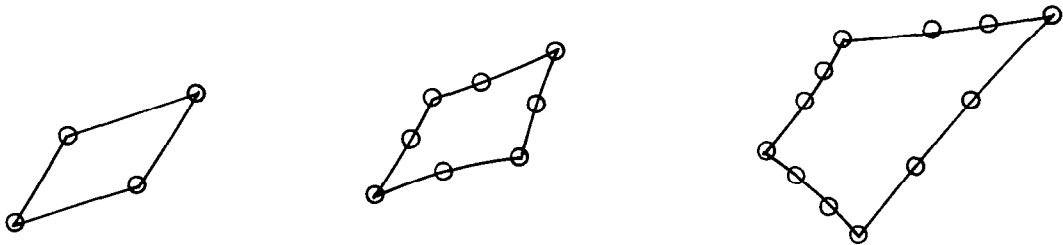
(ϕ modeled at all nodes)

The second program (SUBSON2) uses the tensor product of Hermite polynomials mapped to an irregular region with auxiliary mapping points (denoted by x).
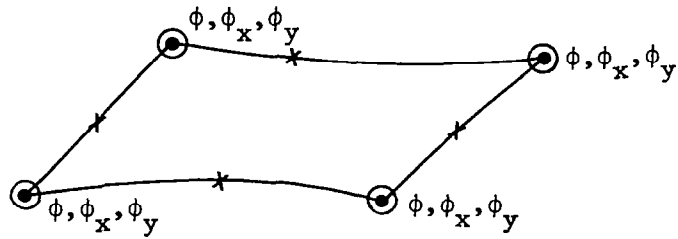
These two codes are based on the following system of routines:
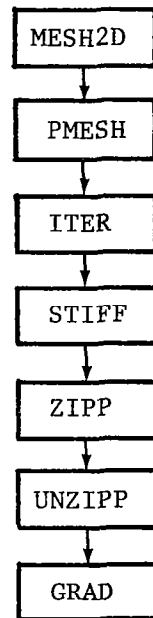
The capabilities of the routines, and, therefore, the program is indicated

in the following descriptions:

    MESH2D   –   Generation of mesh of elements with curvilinear sides

                         for arbitrary domains

PMESH   —   Mesh plot

ITER   —   Iterative driver for solution of subsonic or transonic flow problems

STIFF   —   Generation of matrix equations for each element

ZIPP   —   Frontal solution (direct) routine for a symmetric matrix

UNZIPP   —   Frontal solution (direct) routine for a nonsymmetric matrix

GRAD   —   Computation of the gradients of the solution at the Gauss points

As an example, we computed the incompressible potential flow about a 0.03 parabolic-arc airfoil. In each case, the model contained approximately 600 degrees of freedom. The first model had the four-node serendipity element with 28 elements in the x direction ($x = -1.5$ to $x = 1.5$) and 20 elements in the y direction ($y = 0$ to $y = 2$). There were 12 elements on the airfoil.

As a second example, the same case was computed with the eight-node serendipity element with 18 elements in the x direction ($x = -1.5$ to $x = 1.5$) and 10 elements in the y direction ($y = 0$ to $y = 2$). There were 6 elements on the airfoil.

The solution time for the linear algebraic equations (using the frontal solver) was 30.15 C.P. seconds for the four-node case and 29.44 C.P. seconds for the eight-node case on an IBM 370-158. This time is equivalent to approximately 7.5 C.P. seconds on the CDC 6600 (using a factor of 4 for conversion).

82

Similar runs using line-relaxation methods to solve the same problem (as described

in the section entitled Extensions to the Full Potential Equation) have taken

approximately 7.0 C.P. seconds for 70 relaxation sweeps on the CDC 6600. Thus,

at least for linear problems, the two solution schemes have equivalent computing

times for the moderate-sized examples tested here.

REFERENCES

1. Murman, E. M.; and Cole, J.: AIAA J. 9, no. 1, 1971, pp. 114-121.

2. Martin, E. D.; and Lomax, H.: AIAA Paper No. 74-11, 1974.

3. Jameson, A.: AIAA Second Computational Fluid Dynamics Conference, Hartford, 1975.

4. Sichel, M.: Phys. Fluids 6, 1963, p. 563.

5. Landahl, M. T.: Unsteady Transonic Flow, Pergamon Press, New York, 1961.

6. Keyfitz, B.; Melnik, R.; and Grossman, B.: Grumman Report R5-525, 1976.

7. Sirovich, L.; and Huo, C.: AIAA J. 14, no. 8, 1976.

8. Landau, L. D.: Fluid Mechanics, Pergamon Press, New York, 1959.

9. Guderley, K.: The Theory of Transonic Flows, Pergamon Press, New York, 1962.

10. Zierep, J.; and Oswatitsch, R.: ZAMM 40 supp., T143-144, 1960.

11. Melnik, R.; and Grossman, B.: Symposium Transsonicum II, Gottingen, 1975.

12. Magnus, R.; and Yoshihara, H.: NASA CR-2186, 1973.

13. Murman, E. M.: AIAA J. 12, no. 5, 1974, pp. 626-633.

14. Cheng, H. K.; and Hafez, M. M.: AIAA Paper 73-88, 1973.

15. Cheng, H. K.; and Hafez, M. M.: AIAA Paper 7551, 1975.

16. Caughy, D. A.; and Jameson, A.: AIAA Paper 76100, 1976.

17. Ballhaus, W.; and Steger, J.: NASA TM X-73082, 1975.

18. Brandt, A.; and South, J.: Project SQUID, Monterey, 1976.

19. Yu, N. J.; and Seebass, A. R.: Symposium Transsonicum II, Gottingen, 1975.

20. Warming, R. F.; and Beam, R. M.: AIAA Second Computational Fluid Dynamics Conference, Hartford, 1975.

21. Martin, E.: AIAA Second Computational Fluid Dynamics Conference, Hartford, 1975.

22. Oden, J. T.: Finite Elements of Nonlinear Continua, McGraw Hill, 1972.

23. Wahlbin, L. B.: Mathematical Aspects of Finite Elements, AP. 1974.

24. Kreiss, H. O.; and Scherer, G.: Mathematical Aspects of Finite Element in Partial Differential Equations, Academic Press, New York, 1974.

25. Swartz, B.; and Wendroff, B.: Math. of Comp. 23, no. 105, 1969, pp. 37-49.

26. Carasso, A.: Math. of Comp. 29, no. 130, 1974, pp. 447-463.

27. Carasso, A.: Math. of Comp. 28, no. 127, 1974, pp. 757-767.

28. Mote, C. D.: Int. J. Num. Methods Eng. 3, no. 4, 1971, pp. 565-574.

29. Wang, C. T.: J. Aero, Sci. 17, 1950, p. 343.

30. Weare, T. J.: Comp. Meth. in Appl. Mech. and Engr. 7, 1976, pp. 351-357.

31. Kawahara, M.: Second International Symposium on Finite Element Methods in Flow Problems, 1976.

32. Bauer, F.; Korn, D.; Jameson, A.; and Garabedian, P.: Supercritical Wing Sections, Springer Verlag, New York, 1975.

33. Birkhoff, G.; and Gulati, S.: SIAM J. Num. Analysis 11, no. 4, 1974.

34. Wheeler, M. F.: SIAM J. Num. Analysis 11, no. 4, 1974.

35. Birkhoff, G.; and Dougalis, V. A. (edited by Vichnevetsky, R.): Advances in Computer Methods For Partial Differential Equations, AICA, 1975.

36. Swartz, B. (edited by Vichnevetsky, R.): Advances in Computer Methods For Partial Differential Equations, AICA, 1975.

37. Vichnevetsky, R.; and De Schutter, F.: Advances in Computer Methods For Partial Differential Equations, AICA, 1975, p. 46.

38. Vichnevetsky, R.; and Pfeiffer, B.: Advances in Computer Methods For Partial Differential Equations, AICA, 1975, p. 53.

39. Goudrea, G. L.; and Taylor, R. L.: Comp. Meth. in Appl. Mech. and Engr. 2, 1972, pp. 64-97.

40. Argyris, J. H.; Dunne, P. C.; and Angelopoulos, T.: Comp. Meth. in Appl. Mech. and Engr. 2, 1973, pp. 203-250.

41. Argyris, J. H.; and Scharpf, D. W.: The Aero. J. of the Roy. Aero. Soc., 1969, pp. 1041-1044.

42. Fried, J.: AIAA J. 7, 1170, 1969.

43. Zienkiewicz, O. C.; and Lewis, R. W.: J. of Earthquake Engr., 1972, pp. 407-408.

44. Hafez, M. M.; Murman, E. M.; and Wellford, L. C.: Second International Symposium on Finite Element Methods in Flow Problems, 1976.

45. Chan, S. T. K.; and Brashears, M. R.: AFFDL-TR-74-11 Wright Patterson Air Force Base, Ohio, 1974.

46. Von Neumann, J.; and Lees, M.: J. Soc. Ind. Appl. Math. 10, 1962, p. 610.

47. Showalter, R. W.: SIAM J. Math. Analysis 1, no. 1, 1970.

48. Wellford, L. C.; and Oden, J. T.: J. of Comp. Physics 19, no. 2, 1975, p. 179.

49. Glowinski, R.; and Pironneau, O.: Second International Symposium on Finite Element Methods in Flow Problems, 1976.

50. Wellford, L. C.; and Hafez, M. M.: Second International Symposium on Finite Element Methods in Flow Problems, 1976.
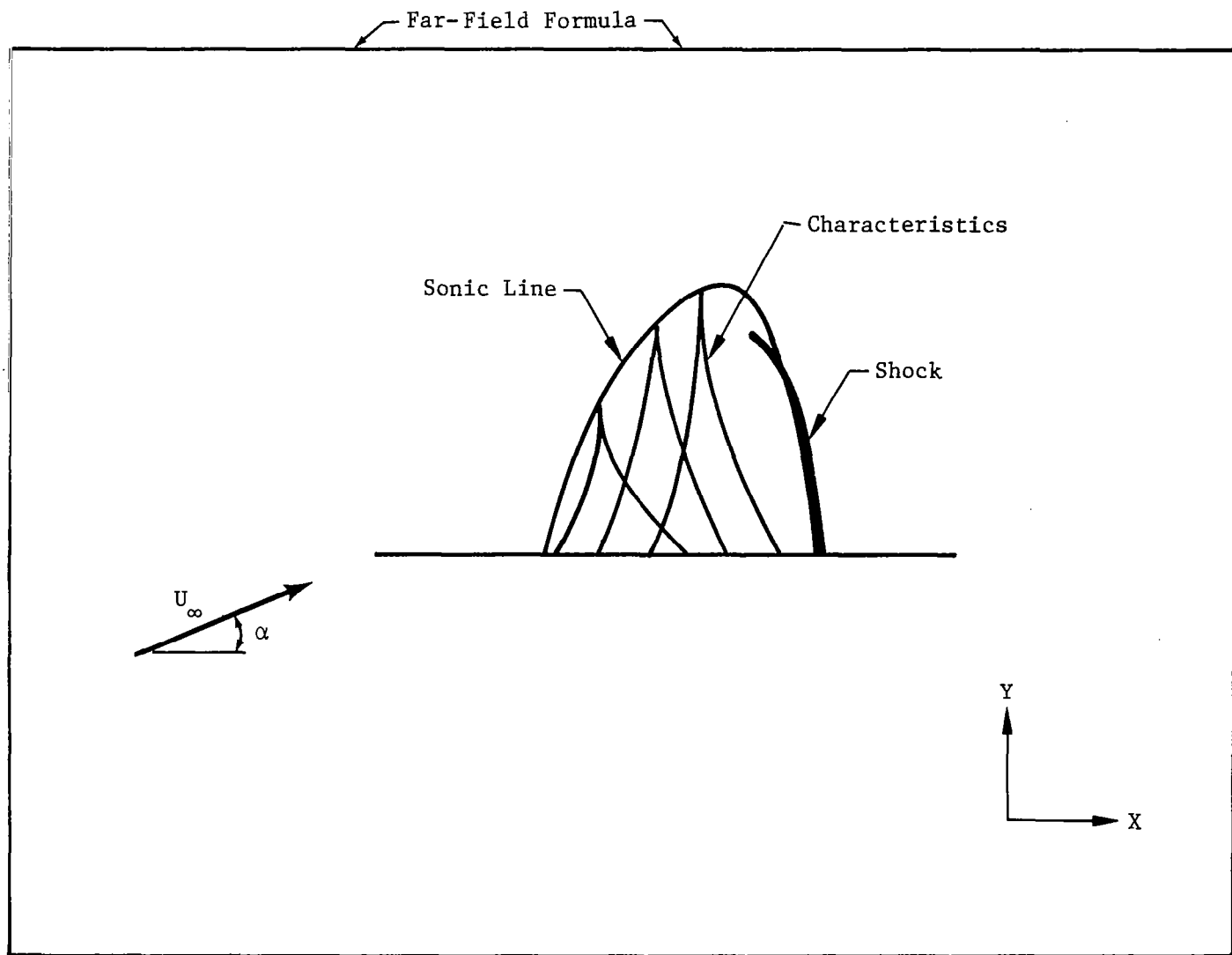
Figure 1. Formulation of Transonic Small-Disturbance Theory
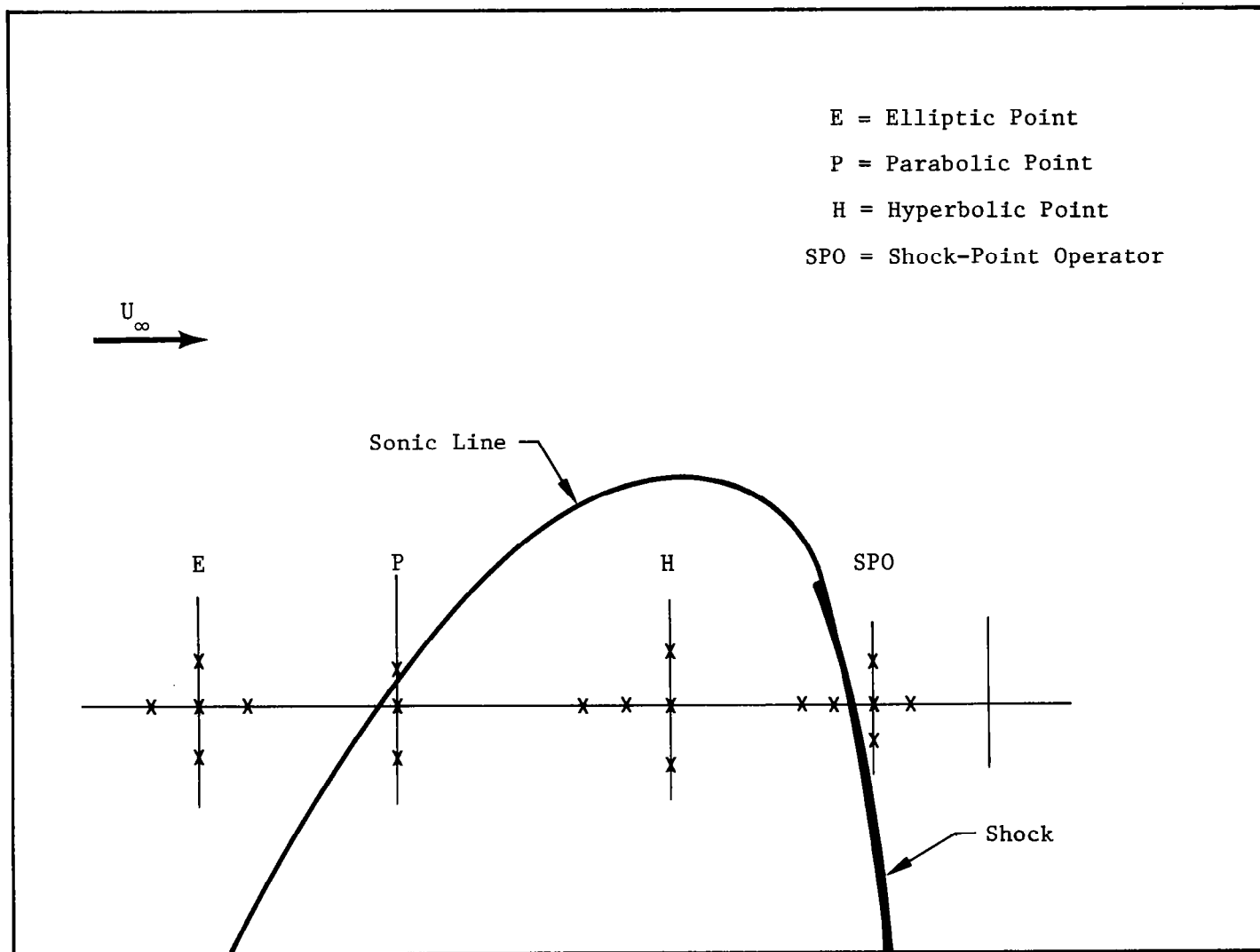
Figure 2. Murman's Fully Conservative Finite-Difference Scheme

Case	Shock-Point Operator	Far Field	LF/TE On Grid Point	Grid Size
A1	Yes	Yes	Between	Std
B1	No	Yes	Between	Std
C1	No	No	Between	Std
D1	No	No	Yes	Dx/2 Dy/2
E1	No	No	Yes	Std
F1	Yes	No	Between	Std
G1	Yes	No	Yes	Std
H1	Yes	No	Yes	Dx/2 Dy/2

Figure 3A   Finite-Difference Solution of Transonic Flow Using Murman's Scheme – Case Identification and Convergence Summary (6% Parabolic Arc Airfoil, $M_\infty = 0.9$)
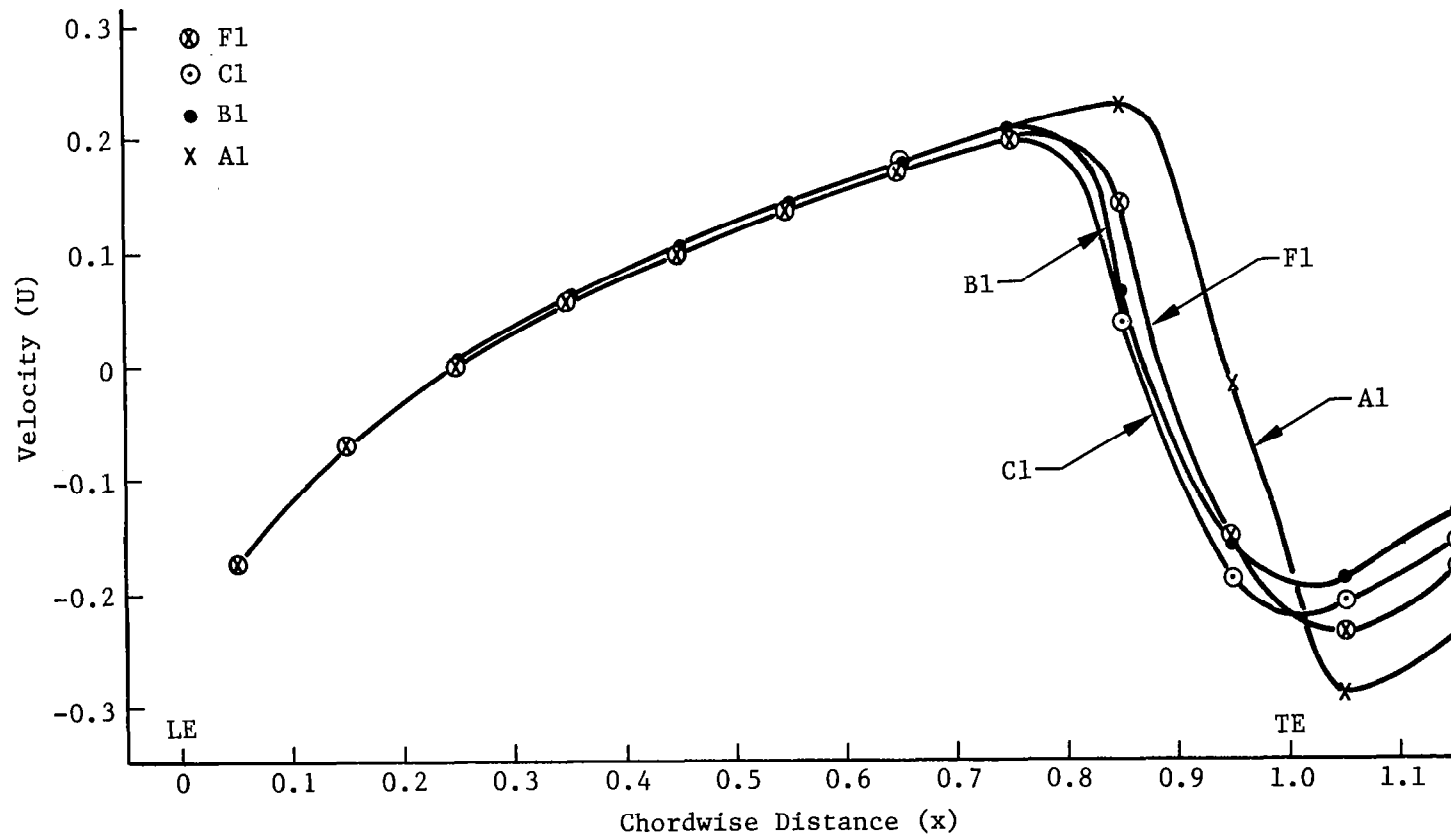
Figure 3B. Finite-Difference Solution of Transonic Flow Based on Murman's Scheme
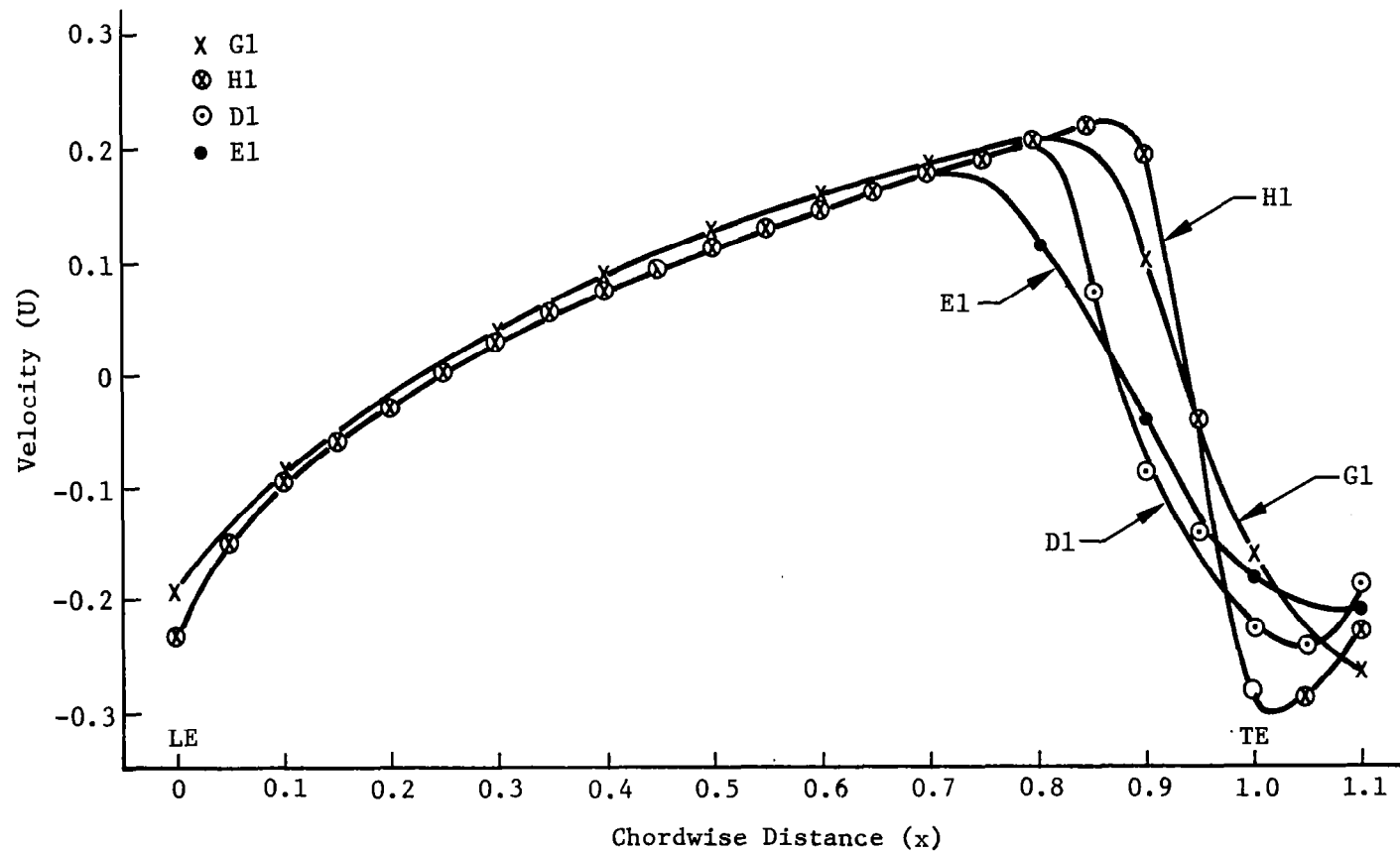
Figure 3C. Finite-Difference Solution of Transonic Flow Based on Murman's Scheme

Dispersive
Dissipative

Dispersive
Non-Dissipative
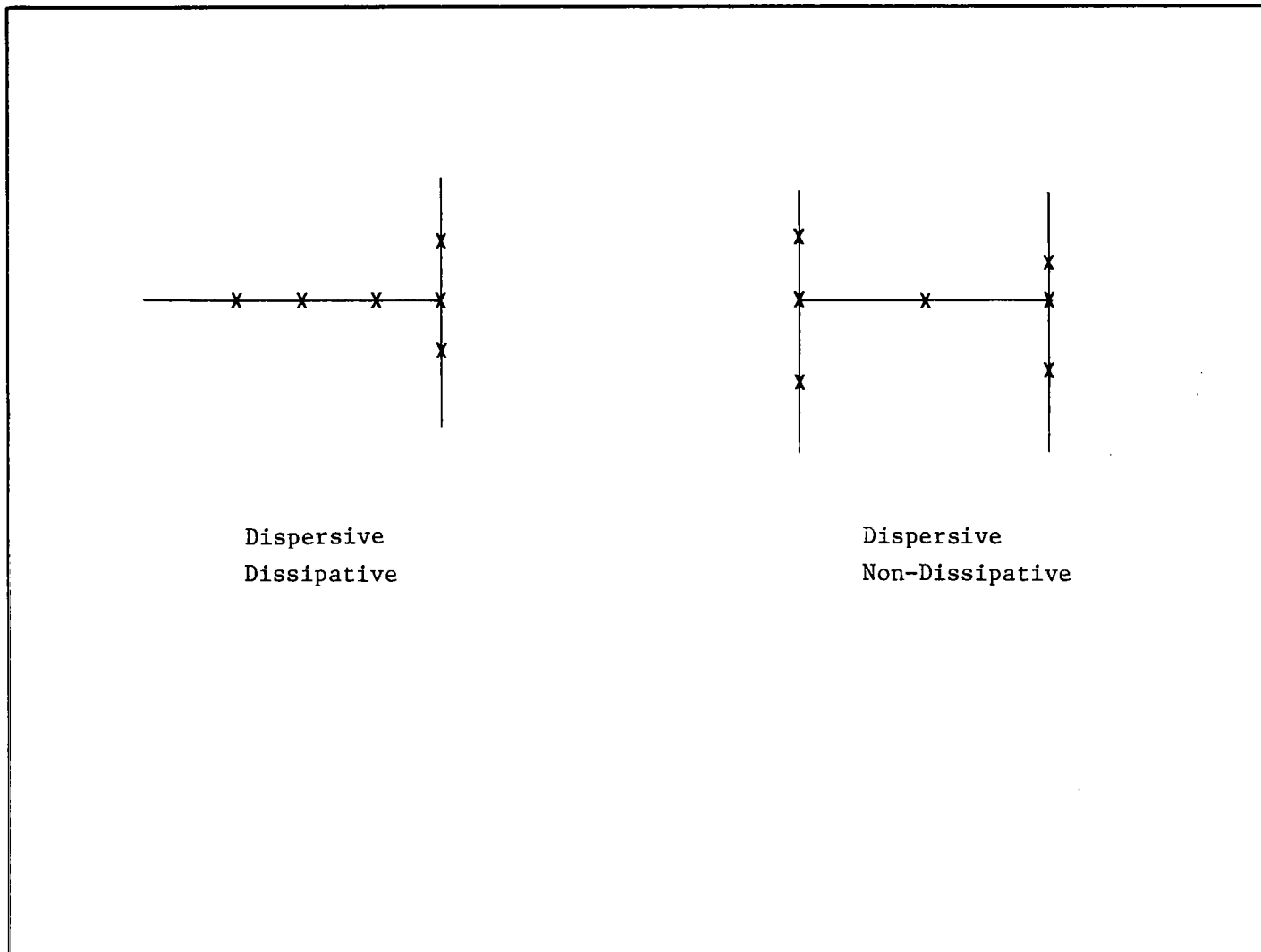
Figure 4A. Implicit, Second-Order-Accurate, Finite-Difference Schemes
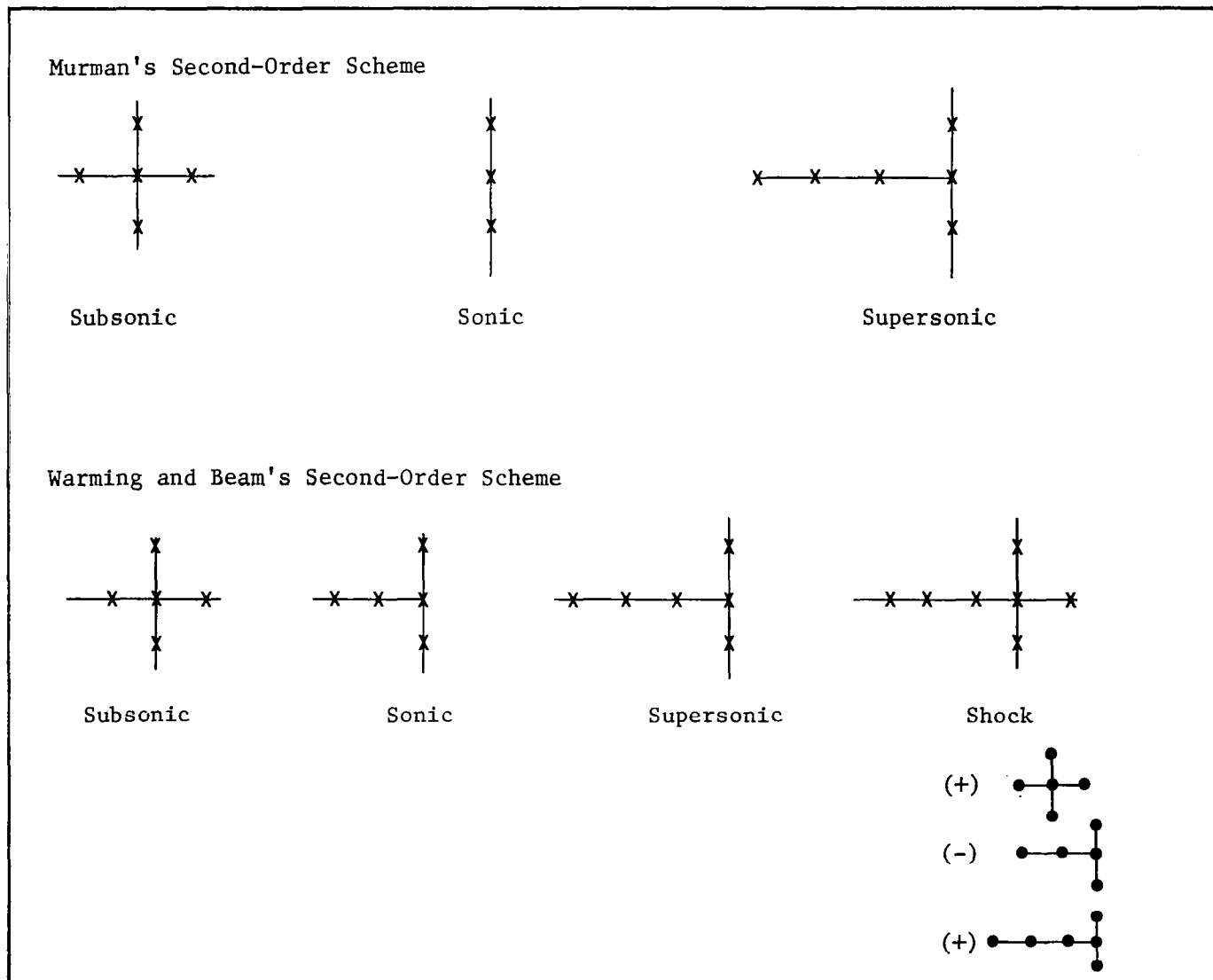
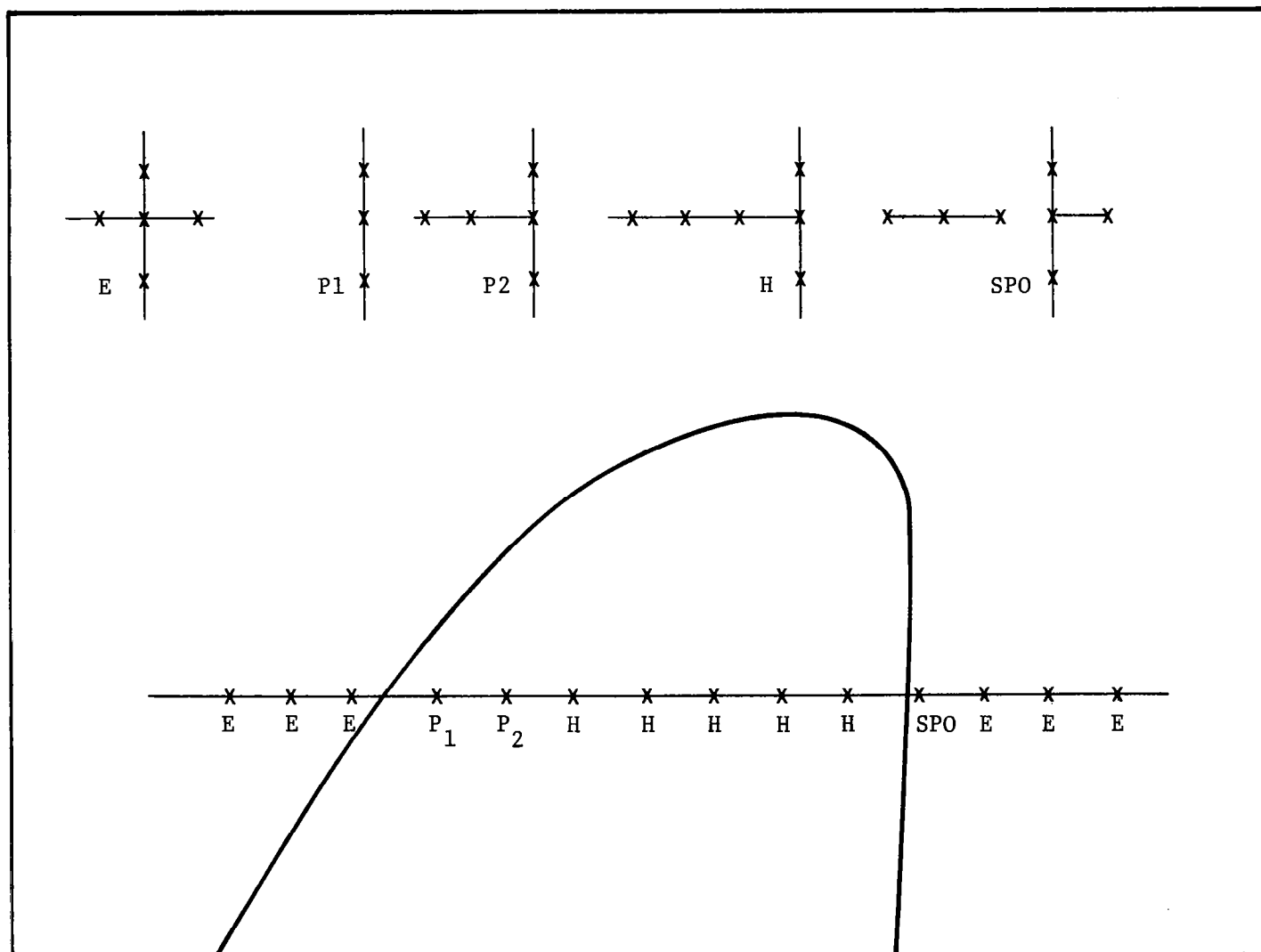Figure 4B. Comparison of Murman's Second-Order Scheme with Warming and Beam's Second-Order Scheme

Figure 4C. Second-Order-Accurate, Fully Conservative Scheme for
Finite-Difference Solution of Transonic Flow

Case	Shock-Point Operator	Far Field	Parabolic Point	Grid Size
A4	Second-Order	No	Two	Std
B4	Second-Order	No	Two	Dx/2 Dy/2
C4	Locally Normal First-Order	No	Two	Std
D4	Locally Normal First-Order	No	Two	Dx/2 Dy/2
E4	First-Order	No	Two	Dx/2 Dy/2
F4	First-Order	No	Two	Std
G4	No	No	Two	Std
H4	No	No	Two	Std
I4	No	No	Murman & Cole (1971)	Std
J4	Warming & Beam (1975)	No	Warming & Beam (1975)	Std

Figure 5A. Second-Order Finite-Difference Solution of Transonic
Flow – Case Identification and Convergence Summary
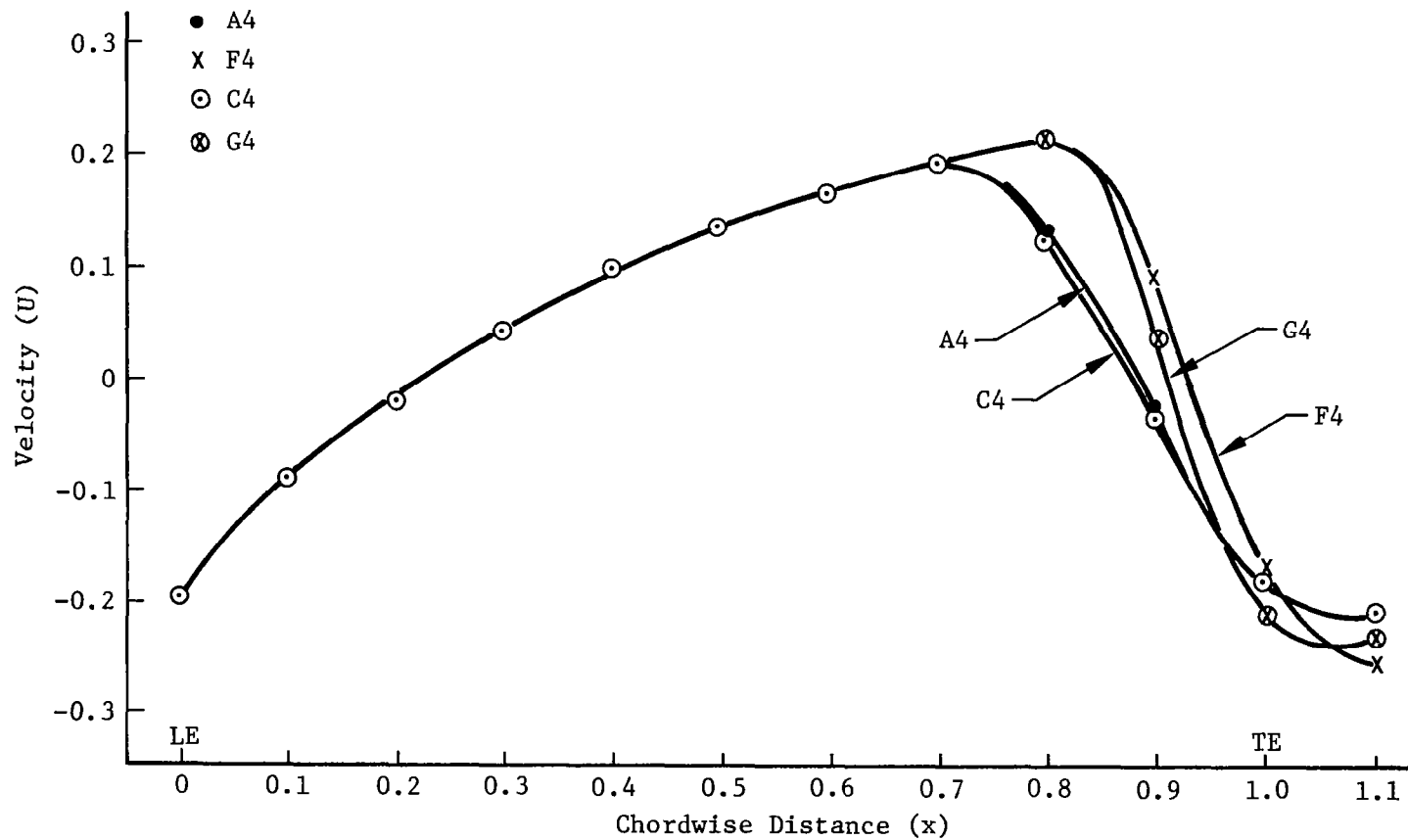
Figure 5B. Second-Order-Accurate, Finite-Difference Solutions For Transonic Flow — Coarse Grid, Showing Effect of Shock Operator
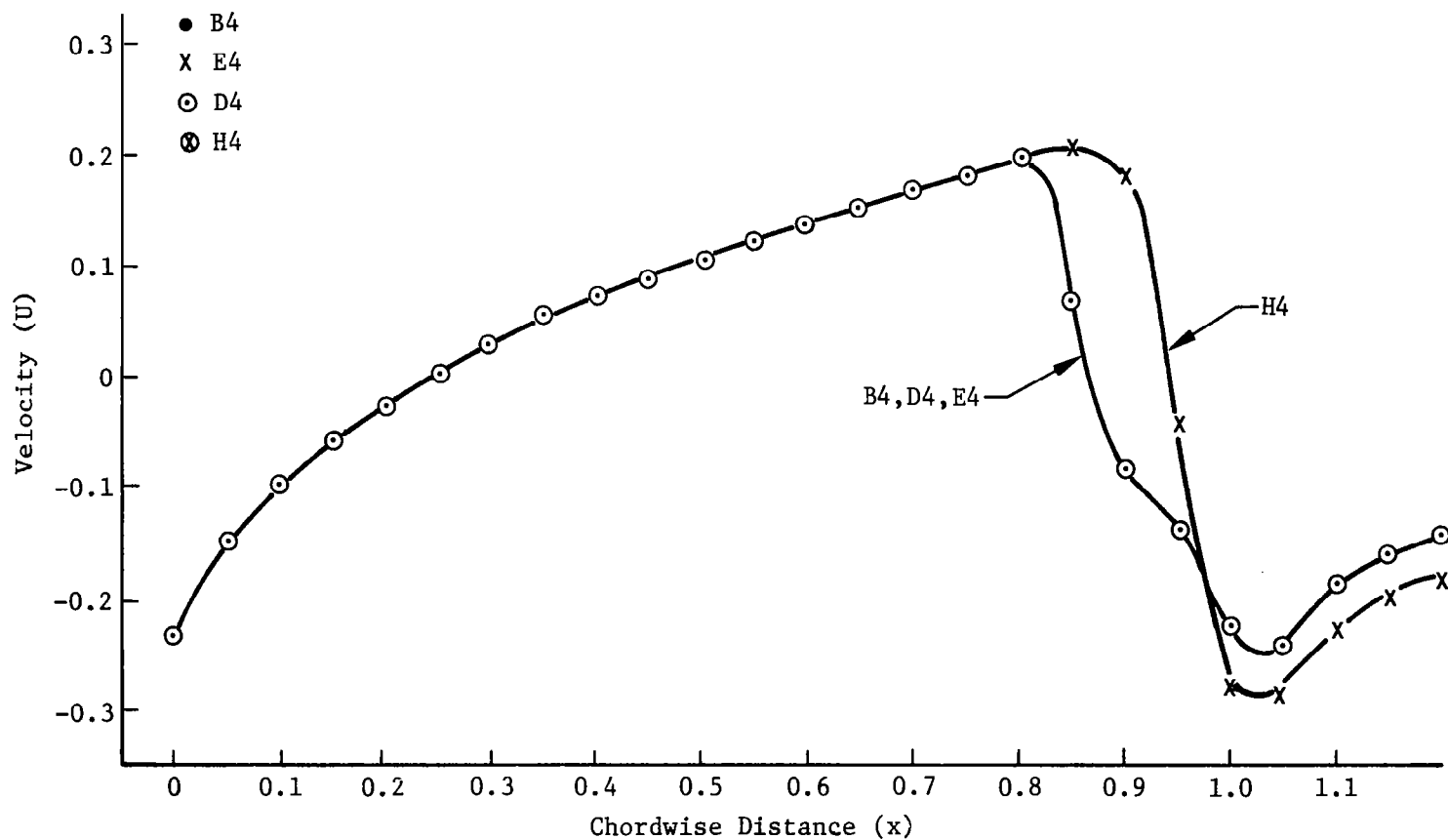
Figure 5C   Second-Order-Accurate, Finite-Difference Solutions
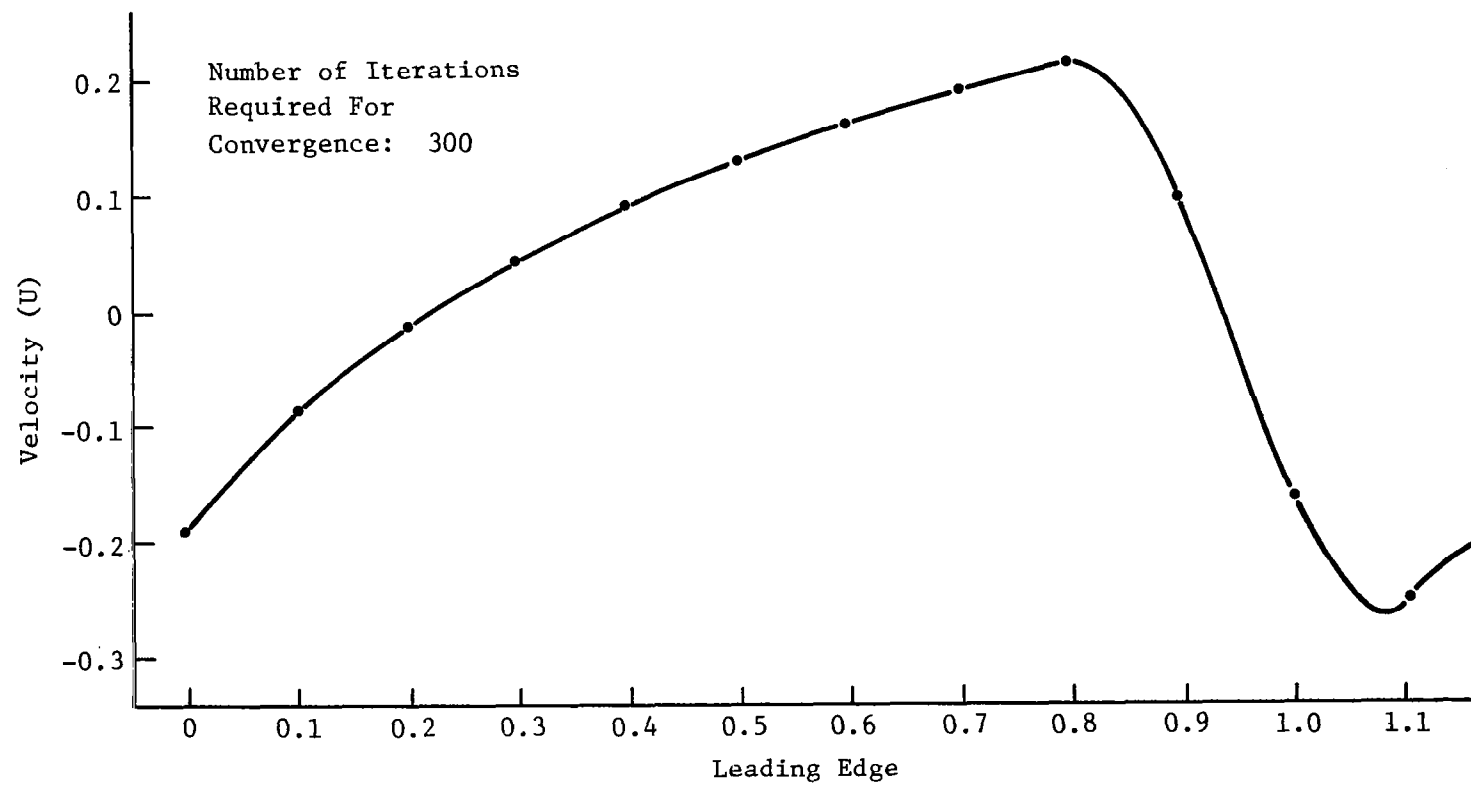for Transonic Flow — Fine Grid

Figure 6. Solution of Transonic Flow by Relaxation of Laplace Operator

Notation

$$\begin{array}{lcc} & \text{X}\!\!-\!\!-\!\!-\!\!-\!\!-\!\!-\!\!\text{X} \\ \phi & 1 & 2 \\ \phi_x & 3 & 4 \end{array}$$

Degree of Freedom #1 (Weighting Function, β_1)

$$\left(\frac{156h}{420} + \frac{36}{30}\right)\chi_1 + \left(\frac{54h}{420} - \frac{36}{30}\right)\chi_2 + \left(\frac{22h^2}{420} + \frac{1}{10}\right)\chi_3 + \left(\frac{-13h^2}{420} + \frac{1}{10}\right)\chi_4$$

Degree of Freedom #2 (Weighting Function, β_2)

$$\left(\frac{54h}{420} - \frac{36}{30}\right)\chi_1 + \left(\frac{156h}{420} + \frac{36}{30}\right)\chi_2 + \left(\frac{13h^2}{420} - \frac{1}{10}\right)\chi_3 + \left(- \frac{22h^2}{420} - \frac{1}{10}\right)\chi_4$$

Degree of Freedom #3 (Weighting Function, β_3)

$$\left(\frac{22h^2}{420} - \frac{1}{10}\right)\chi_1 + \left(\frac{13h^2}{420} - \frac{1}{10}\right)\chi_2 + \left(\frac{4h^3}{420} + \frac{4h}{30}\right)\chi_3 + \left(- \frac{3h^3}{420} - \frac{h}{30}\right)\chi_4$$

Degree of Freedom #4 (Weighting Function, β_4)

$$\left(\frac{-13h^2}{420} + \frac{1}{10}\right)\chi_1 + \left(- \frac{22h^2}{420} - \frac{1}{10}\right)\chi_2 + \left(- \frac{3h^3}{420} - \frac{h}{30}\right)\chi_3 + \left(\frac{4h^3}{420} + \frac{4h}{30}\right)\chi_4$$

Figure 7. Influence Coefficients for the Four Degrees of Freedom
in a Hermitian Cubic Element

Coefficient Of . . .	X_1	X_2	X_3	X_4	X_5	X_6
Galerkin Formulation	$\frac{54h}{420} - \frac{36}{30}$	$\frac{156h}{420} + \frac{36}{30}$ $\frac{156h}{420} + \frac{36}{30}$	$\frac{54h}{420} - \frac{36}{30}$	$\frac{13h^2}{420} - \frac{1}{10}$	$-\frac{22h^2}{420} - \frac{1}{10}$ $\frac{22h^2}{420} + \frac{1}{10}$	$\frac{-13h^2}{420} + \frac{1}{10}$
Hamiltonian Formulation	Same as Galerkin					
Least-Squares Formulation	$-\frac{12}{h^3} - \frac{12}{5h}$ $+ \frac{54h}{420}$	$\frac{12}{h^3} + \frac{12}{5h}$ $+ \frac{156h}{420}$ $\frac{12}{h^3} + \frac{12}{5h}$ $+ \frac{156h}{420}$	$-\frac{12}{h^3} - \frac{12}{5h}$ $+ \frac{54h}{420}$	$\frac{-6}{h^2} - \frac{1}{5}$ $+ \frac{13h^2}{420}$	$\frac{-6}{h^2} - \frac{6}{5}$ $- \frac{22h^2}{420}$ $\frac{6}{h^2} + \frac{6}{5}$ $+ \frac{22h^2}{420}$	$\frac{6}{h^2} + \frac{1}{5}$ $\frac{-13h^2}{420}$

Figure 8A.   Comparison of Influence Coefficients For the ϕ Term (Degree of Freedom Number Two) For the Galerkin, Hamiltonian, and Least-Squares Approaches (Nomenclature Is Defined in the Text)

Coefficient Of . . .	X_1	X_2	X_3	X_4	X_5	X_6
Galerkin Formulation	$\dfrac{-13h^2}{420} + \dfrac{1}{10}$	$\dfrac{-22h^2}{420} - \dfrac{1}{10} +$ $\dfrac{22h^2}{420} + \dfrac{1}{10}$	$\dfrac{13h^2}{420} - \dfrac{1}{10}$	$\dfrac{-3h^3}{420} - \dfrac{h}{30}$	$\dfrac{4h^3}{420} + \dfrac{4h}{30} +$ $\dfrac{4h^3}{420} + \dfrac{4h}{30}$	$\dfrac{-3h^3}{420} - \dfrac{h}{30}$
Hamiltonian Formulation	Same as Galerkin					
Least-Squares Formulation	$\dfrac{6}{h^2} + \dfrac{1}{5}$ $\dfrac{-13h^2}{420}$	$\dfrac{-6}{h^2} - \dfrac{6}{5}$ $\dfrac{-22h^2}{420}$ $+$ $\dfrac{6}{h^2} + \dfrac{6}{5}$ $+ \dfrac{22h^2}{420}$	$\dfrac{-6}{h^2} - \dfrac{1}{5}$ $+ \dfrac{13h^2}{420}$	$\dfrac{2}{h} - \dfrac{h}{15}$ $\dfrac{-3h^3}{420}$	$\dfrac{4}{h} + \dfrac{4h}{15}$ $+ \dfrac{4h^3}{420}$ $+$ $\dfrac{4}{h} + \dfrac{4h}{15}$ $+ \dfrac{4h^3}{420}$	$\dfrac{2}{h} - \dfrac{h}{15}$ $- \dfrac{3h^3}{420}$

Figure 8B. Comparison of Influence Coefficients For the ϕ_x Term (Degree of Freedom Number Five) For the Galerkin, Hamiltonian, and Least-Squares Approaches (Nomenclature Is Defined in the Text)

Subsonic Case (IVP); Coefficients for ϕ

Coefficient Of . . .	X_1	X_2	X_3	X_4	X_5	X_6
Galerkin Formulation	$\dfrac{54h}{420} - \dfrac{36}{30}$	$\dfrac{156h}{420} + \dfrac{36}{30}$	0	$\dfrac{13h^2}{420} - \dfrac{1}{10}$	$\dfrac{-22h^2}{420} - \dfrac{1}{10}$ -1	0
Hamiltonian Formulation	Hamiltonian Influence Coefficients are Determined From Two ϕ_{xx} Terms (See Fig. 8B)					
Least-Squares Formulation	$\dfrac{6}{h^2} + \dfrac{1}{5}$ $-\dfrac{13h^2}{420}$	$\dfrac{-6}{h^2} - \dfrac{6}{5}$ $-\dfrac{22h^2}{420}$	0	$\dfrac{2}{h} - \dfrac{h}{15}$ $-\dfrac{3h^3}{420}$	$\dfrac{4}{h} + \dfrac{4h}{15}$ $+\dfrac{4h^3}{420}$	0

Figure 9A. Comparison of Influence Coefficients For the ϕ Term For the Galerkin, Hamiltonian and Least-Squares Formulations - Supersonic Case (Nomenclature Is Defined in the Text)

Supersonic Case (IVP); Coefficients for ϕ_x

Coefficient Of . . .	χ_1	χ_2	χ_3	χ_4	χ_5	χ_6
Galerkin Formulation	$\dfrac{-13h^2}{420} + \dfrac{1}{10}$	$\dfrac{-22h^2}{420} - \dfrac{1}{10}$	0	$\dfrac{-3h^3}{420} - \dfrac{h}{30}$	$\dfrac{4h^3}{420} + \dfrac{4h}{30}$	0
Hamiltonian Formulation	* $\dfrac{-13h^2}{420} + \dfrac{1}{10}$	$\dfrac{-22h^2}{420} - \dfrac{1}{10}$	0	$\dfrac{-3h^3}{420} - \dfrac{h}{30}$	$\dfrac{4h^3}{420} + \dfrac{4h}{30}$	0
	** $\dfrac{22h^2}{420} + \dfrac{1}{10}$	$\dfrac{13h^2}{420} - \dfrac{1}{10}$	0	$\dfrac{4h^3}{420} + \dfrac{4h}{30}$	$\dfrac{-3h^3}{420} - \dfrac{h}{30}$	0
Least-Squares Formulation	$\dfrac{6}{h^2} + \dfrac{6}{5}$ $+ \dfrac{22h^2}{420}$	$\dfrac{-6}{h^2} - \dfrac{1}{5}$ $+ \dfrac{13h^2}{420}$	0	$\dfrac{4}{h} + \dfrac{4h}{15}$ $+ \dfrac{4h^3}{420}$	$\dfrac{2}{h} - \dfrac{h}{15}$ $- \dfrac{3h^3}{420}$	0

*This row obtained by weighting at point 5

**This row obtained by weighting at point 4

Figure 9B.   Comparison of the Influence Coefficients For the ϕ_x Term For Galerkin, Hamiltonian, and Least-Squares Formulations - Supersonic Case (Nomenclature Is Defined in the Text)

Galerkin or Hamiltonian Influence Coefficients For ϕ

Point No.	1	2	3	4	5	6	7	8	9	10	11	12	13	14	15	16	17	18
Contribution From Element A	$-\frac{\alpha_1}{5}$ $+\frac{9}{70}$	$\frac{\alpha_1}{5}$ $+\frac{13}{35}$		$-\frac{2\alpha_1}{5}$ $+\frac{9}{70}$	$\frac{3\alpha_1}{5}$ $-\frac{13}{35}$					$-\frac{\alpha_1 h}{60}$ $+\frac{13h}{420}$	$-\frac{\alpha h}{60}$ $-\frac{11h}{420}$		$-\frac{\alpha_1 h}{30}$ $-\frac{13h}{420}$	$-\frac{\alpha_1 h}{30}$ $+\frac{11h}{210}$				
Contribution From Element B		$+\frac{\alpha_2}{5}$ $+\frac{13}{35}$	$-\frac{\alpha_2}{5}$ $+\frac{9}{70}$		$+\frac{2\alpha_2}{5}$ $-\frac{13}{35}$	$-\frac{2\alpha_2}{5}$ $-\frac{9}{70}$					$+\frac{\alpha_2 h}{60}$ $+\frac{22h}{420}$	$\frac{\alpha_2 h}{60}$ $-\frac{13h}{420}$		$\frac{\alpha_2 h}{30}$ $-\frac{11h}{210}$	$\frac{\alpha_2 h}{30}$ $+\frac{13h}{420}$			
Contribution From Element C				$-\frac{2\alpha_3}{5}$ $-\frac{9}{70}$	$+\frac{2\alpha_3}{5}$ $-\frac{13}{35}$		$-\frac{\alpha_3}{5}$ $+\frac{9}{70}$	$+\frac{\alpha_3}{5}$ $+\frac{13}{35}$					$-\frac{\alpha_3 h}{30}$ $-\frac{13h}{420}$	$-\frac{\alpha_3 h}{30}$ $+\frac{11h}{210}$		$-\frac{\alpha_3 h}{60}$ $+\frac{13h}{420}$	$-\frac{\alpha_3 h}{60}$ $-\frac{11h}{210}$	
Contribution From Element D					$+\frac{2\alpha_4}{5}$ $-\frac{13}{35}$	$-\frac{2\alpha_4}{5}$ $-\frac{9}{70}$		$\frac{\alpha_4}{5}$ $+\frac{13}{35}$	$-\frac{\alpha_4}{5}$ $+\frac{9}{70}$					$\frac{\alpha_4 h}{30}$ $-\frac{11h}{210}$	$\frac{\alpha_4 h}{30}$ $+\frac{13h}{420}$		$\frac{\alpha_4 h}{60}$ $+\frac{11h}{210}$	$\frac{\alpha_4 h}{60}$ $-\frac{13h}{420}$

Note: Influence Coefficient For Each Point Is the Sum of All Terms in That Column
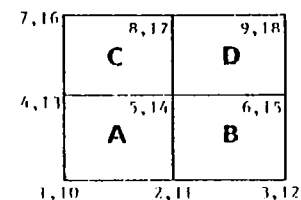
Figure 10A. Influence Coefficients For Galerkin and Hamiltonian
Influence Coefficients – Subsonic Case For ϕ Term

Galerkin or Hamiltonian Influence Coefficients For ϕ_x

Point No.	1	2	3	4	5	6	7	8	9	10	11	12	13	14	15	16	17	18
Contribution From Element A	$\frac{\alpha_1 h}{60}$ $-\frac{13h}{420}$	$-\frac{\alpha_1 h}{60}$ $-\frac{11h}{210}$		$\frac{\alpha_1 h}{30}$ $+\frac{13h}{420}$	$-\frac{\alpha_1 h}{30}$ $+\frac{11h}{210}$					$-\frac{\alpha_1 h^2}{180}$ $-\frac{h^2}{105}$	$\frac{\alpha_1 h^2}{45}$ $+\frac{h^2}{105}$		$-\frac{\alpha_1 h^2}{90}$ $+\frac{h^2}{105}$	$\frac{2\alpha_1 h^2}{45}$ $-\frac{h^2}{105}$				
Contribution From Element B		$\frac{\alpha_2 h}{60}$ $+\frac{11h}{210}$	$-\frac{\alpha_2 h}{60}$ $+\frac{13h}{420}$		$\frac{\alpha_2 h}{30}$ $-\frac{11h}{210}$	$-\frac{\alpha_2 h}{30}$ $-\frac{13h}{420}$					$\frac{\alpha_2 h^2}{45}$ $+\frac{h^2}{105}$	$\frac{\alpha_2 h^2}{180}$ $-\frac{h^2}{105}$		$\frac{2\alpha_2 h^2}{45}$ $-\frac{h^2}{105}$	$-\frac{\alpha_2 h^2}{90}$ $+\frac{h^2}{105}$			
Contribution From Element C				$\frac{\alpha_3 h}{30}$ $+\frac{13h}{420}$	$-\frac{\alpha_3 h}{30}$ $+\frac{11h}{420}$		$\frac{\alpha_3 h}{60}$ $-\frac{13h}{420}$	$-\frac{\alpha_3 h}{60}$ $-\frac{11h}{210}$					$-\frac{\alpha_3 h^2}{90}$ $+\frac{h^2}{105}$	$\frac{2\alpha_3 h^2}{45}$ $-\frac{h^2}{105}$		$-\frac{\alpha_3 h^2}{180}$ $-\frac{h^2}{105}$	$\frac{\alpha_3 h^2}{45}$ $+\frac{h^2}{105}$	
Contribution From Element D					$\frac{\alpha_4 h}{30}$ $-\frac{11h}{210}$	$-\frac{\alpha_4 h}{30}$ $-\frac{13h}{420}$		$\frac{\alpha_4 h}{60}$ $+\frac{11h}{210}$	$-\frac{\alpha_4 h}{60}$ $+\frac{h}{420}$					$\frac{2\alpha_4 h}{45}$ $-\frac{h^2}{105}$	$-\frac{\alpha_4 h^2}{90}$ $+\frac{h^2}{105}$		$\frac{\alpha_4 h^2}{45}$ $+\frac{h^2}{105}$	$-\frac{\alpha h^2}{180}$ $-\frac{h^2}{105}$

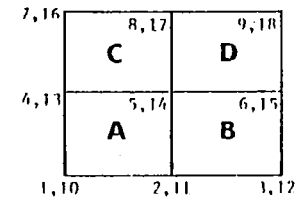Note: Influence Coefficient For Each Point Is the Sum of All Terms in That Column

Figure 10B. Influence Coefficients For Galerkin and Hamiltonian Formulations – Subsonic Case For ϕ_x Term

Hamiltonian Influence Coefficients For ϕ_x — Supersonic

Point No.	1	2	3	4	5	6	7	8	9	10	11	12	13	14	15	16	17	18
Contribution From Element A	$\dfrac{\alpha_1 h}{60}$ $-\dfrac{13h}{420}$	$-\dfrac{\alpha_1 h}{60}$ $-\dfrac{11h}{420}$		$\dfrac{\alpha_1 h}{30}$ $+\dfrac{13h}{420}$	$-\dfrac{\alpha_1 h}{30}$ $+\dfrac{11h}{210}$					$\dfrac{-\alpha_1 h^2}{180}$ $-\dfrac{h^2}{105}$	$\dfrac{\alpha_1 h^2}{45}$ $+\dfrac{h^2}{105}$		$\dfrac{-\alpha_1 h^2}{90}$ $+\dfrac{h^2}{105}$	$\dfrac{2\alpha_1 h^2}{45}$ $-\dfrac{h^2}{105}$				
Contribution From Element B						No Contribution From Element B												
Contribution From Element C				$\dfrac{\alpha_3 h}{30}$ $+\dfrac{13h}{420}$	$\dfrac{\alpha_3 h}{30}$ $+\dfrac{11h}{210}$		$\dfrac{\alpha_3 h}{60}$ $-\dfrac{13h}{420}$	$\dfrac{-\alpha_3 h}{60}$ $-\dfrac{11h}{420}$					$\dfrac{-\alpha_3 h^2}{90}$ $+\dfrac{h^2}{105}$	$\dfrac{2\alpha_3 h^2}{45}$ $-\dfrac{h^2}{105}$		$\dfrac{-\alpha_3 h^2}{180}$ $-\dfrac{h^2}{105}$	$\dfrac{\alpha_3 h^2}{45}$ $+\dfrac{h^2}{105}$	
Contribution From Element D						No Contribution From Element D												

Note: Influence Coefficient For Each Point Is the Sum of All Terms in That Column

7,16		8,17		9,18
	C		D	
4,13		5,14		6,15
	A		B	
1,10		2,11		3,12

Figure 11A. Influence Coefficients For the Hamiltonian Formulation —
Supersonic Case For the ϕ_x Term Weighted at Point 14

Hamiltonian Influence Coefficients For ϕ_x — Supersonic

Point No.	1	2	3	4	5	6	7	8	9	10	11	12	13	14	15	16	17	18
Contribution From Element A	$\frac{\alpha_1 h}{60}$ $+\frac{11h}{210}$	$\frac{-\alpha_1 h}{60}$ $+\frac{13h}{420}$		$\frac{\alpha_1 h}{30}$ $-\frac{11h}{210}$	$\frac{\alpha_1 h}{30}$ $+\frac{13h}{420}$					$\frac{\alpha_1 h^2}{45}$ $+\frac{h^2}{105}$	$\frac{-\alpha_1 h^2}{180}$ $-\frac{h^2}{105}$		$\frac{2\alpha_1 h^2}{45}$ $-\frac{h^2}{105}$	$\frac{-\alpha_1 h^2}{90}$ $+\frac{h^2}{105}$				
Contribution From Element B							No Contribution From Element B											
Contribution From Element C				$\frac{\alpha_3 h}{30}$ $-\frac{11h}{210}$	$\frac{-\alpha_3 h}{30}$ $-\frac{13h}{420}$		$\frac{\alpha_3 h}{60}$ $+\frac{11h}{210}$	$\frac{-\alpha_3 h}{60}$ $+\frac{13h}{420}$					$\frac{2\alpha_3 h}{45}$ $-\frac{h^2}{105}$	$\frac{-\alpha_3 h}{90}$ $+\frac{h^2}{105}$		$\frac{\alpha_3 h^2}{45}$ $+\frac{h^2}{105}$	$\frac{-\alpha_3 h^2}{180}$ $-\frac{h^2}{105}$	
Contribution From Element D							No Contribution From Element D											

Note: Influence Coefficient For Each Point Is the Sum of All Terms in That Column

Figure 11B. Influence Coefficients For the Hamiltonian Formulation—
Supersonic Case For the ϕ_x Term Weighted at Point 13

Galerkin Influence Coefficients For ϕ Term — Supersonic

Point No.	1	2	3	4	5	6	7	8	9	10	11	12	13	14	15	16	17	18
Contribution From Element A	$-\frac{\alpha_1}{5}$ $+\frac{9}{70}$	$\frac{\alpha_1}{5}$ $+\frac{13}{35}$		$-\frac{2\alpha_1}{5}$ $-\frac{9}{70}$	$\frac{3\alpha_1}{5}$ $-\frac{13}{35}$					$-\frac{\alpha_1 h}{60}$ $+\frac{13h}{420}$	$\frac{\alpha_1 h}{60}$ $-\frac{11h}{210}$ $+\frac{\alpha h}{6}$		$-\frac{\alpha_1 h}{30}$ $-\frac{13h}{420}$	$-\frac{\alpha_1 h}{30}$ $+\frac{11h}{210}$ $+\frac{\alpha h}{3}$				
Contribution From Element B							No Contribution From Element B											
Contribution From Element C				$-\frac{2\alpha_3}{5}$ $-\frac{9}{70}$	$\frac{2\alpha_3}{5}$ $-\frac{13}{35}$		$-\frac{\alpha_3}{5}$ $+\frac{9}{70}$	$\frac{\alpha_3}{5}$ $+\frac{13}{35}$					$-\frac{\alpha_3 h}{30}$ $-\frac{13h}{420}$	$-\frac{\alpha_3 h}{30}$ $+\frac{11h}{210}$ $+\frac{\alpha h}{3}$		$-\frac{\alpha_3 h}{60}$ $+\frac{13h}{420}$	$-\frac{\alpha_3 h}{60}$ $-\frac{11h}{210}$ $+\frac{\alpha h}{6}$	
Contribution From Element D							No Contribution From Element D											

Note: Influence Coefficient For Each Point Is the Sum of All Terms in That Column

Figure 12A. Influence Coefficients For Galerkin Formulation—
Supersonic Case For ϕ Term

Galerkin Influence Coefficients For ϕ_x Term — Supersonic

Point No.	1	2	3	4	5	6	7	8	9	10	11	12	13	14	15	16	17	18
Contribution From Element A	$\dfrac{\alpha_1 h}{60}$ $-\dfrac{13h}{420}$	$-\dfrac{\alpha_1 h}{60}$ $-\dfrac{11h}{210}$		$\dfrac{\alpha_1 h}{30}$ $+\dfrac{13h}{420}$	$-\dfrac{\alpha_1 h}{30}$ $+\dfrac{11h}{210}$					$-\dfrac{\alpha_1 h^2}{180}$ $-\dfrac{h^2}{105}$	$\dfrac{\alpha_1 h^2}{45}$ $+\dfrac{h^2}{105}$		$-\dfrac{\alpha_1 h^2}{90}$ $+\dfrac{h^2}{105}$	$\dfrac{2\alpha_1 h^2}{45}$ $-\dfrac{h^2}{105}$				
Contribution From Element B							No Contribution From Element B											
Contribution From Element C				$\dfrac{\alpha_3 h}{30}$ $+\dfrac{13h}{420}$	$-\dfrac{\alpha_3 h}{30}$ $+\dfrac{11h}{210}$		$\dfrac{\alpha_3 h}{60}$ $-\dfrac{13h}{420}$	$-\dfrac{\alpha_3 h}{60}$ $-\dfrac{11h}{210}$					$-\dfrac{\alpha_3 h^2}{90}$ $+\dfrac{h^2}{105}$	$\dfrac{2\alpha_3 h^2}{45}$ $-\dfrac{h^2}{105}$		$-\dfrac{\alpha_3 h^2}{180}$ $-\dfrac{h^2}{105}$	$\dfrac{\alpha_3 h^2}{45}$ $+\dfrac{h^2}{105}$	
Contribution From Element D							No Contribution From Element D											

Note: Influence Coefficient For Each Point is the Sum of All Terms in That Column

Figure 12B. Influence Coefficients For the Galerkin Formulation—
Supersonic Case For ϕ_x Term
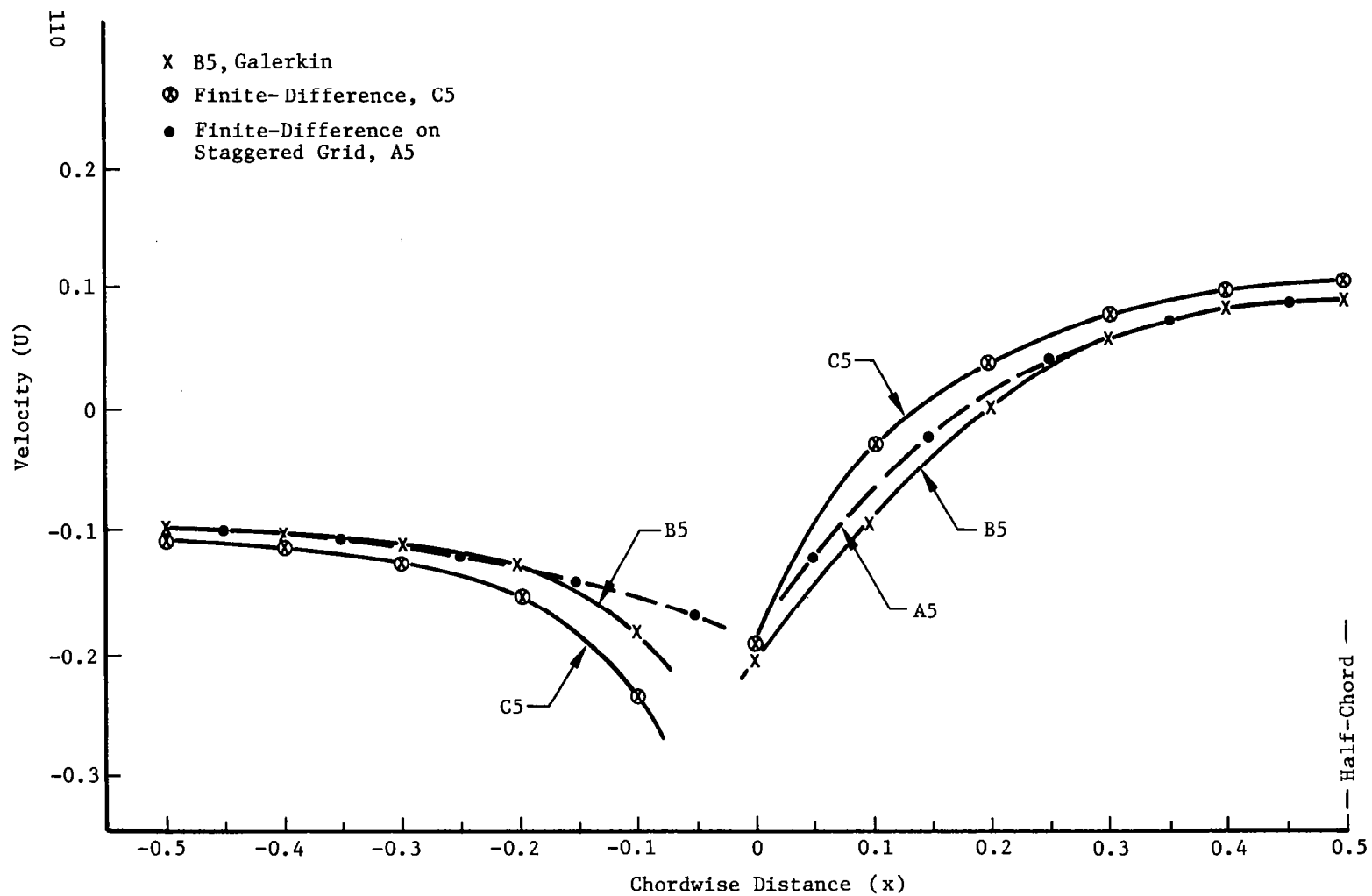
Figure 13A   Comparison of the Galerkin Method With the Finite-Difference
Method For Incompressible Flow
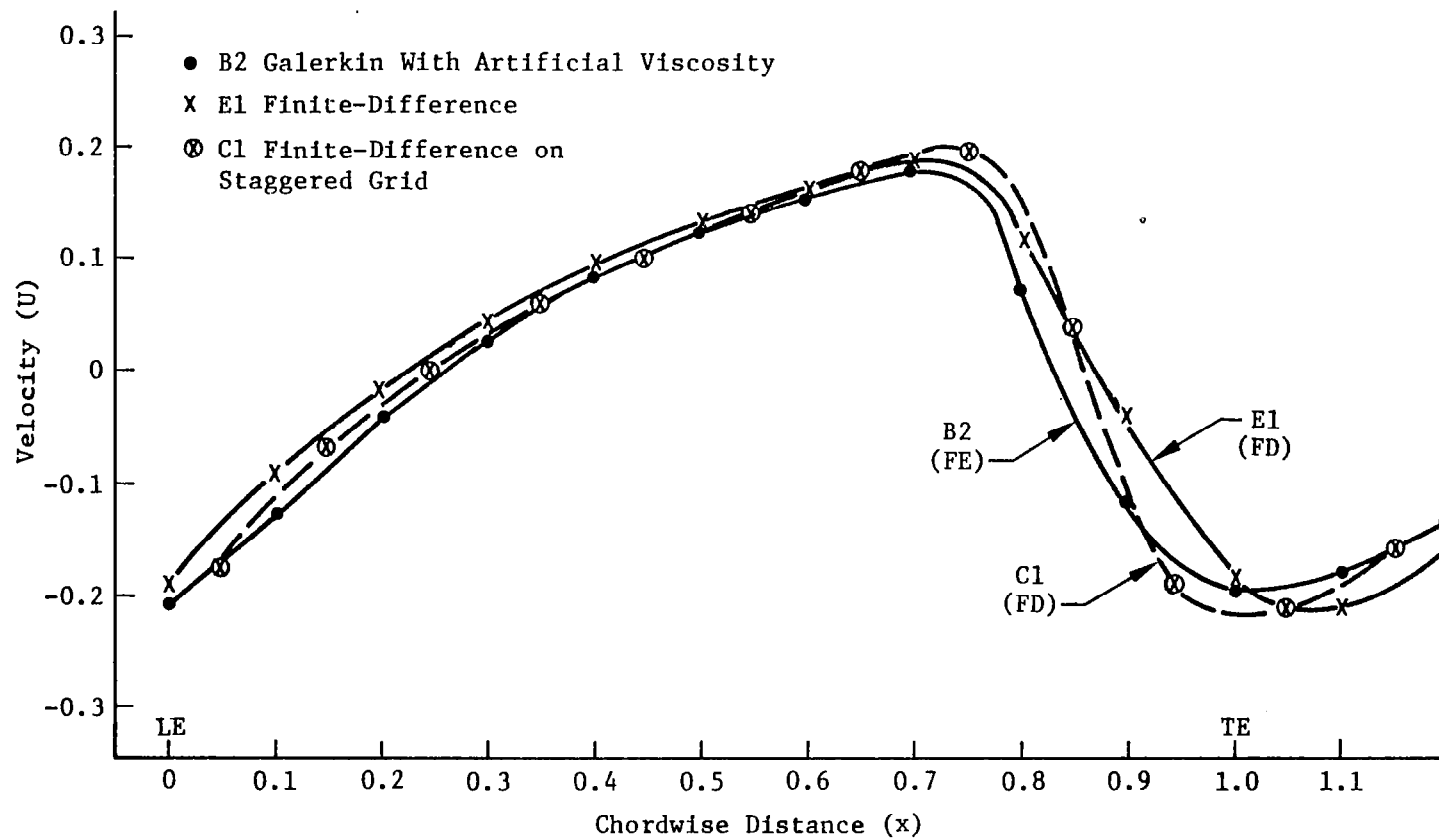
Figure 13B. Comparison of Finite-Element and Finite-Difference Results For Transonic Flow
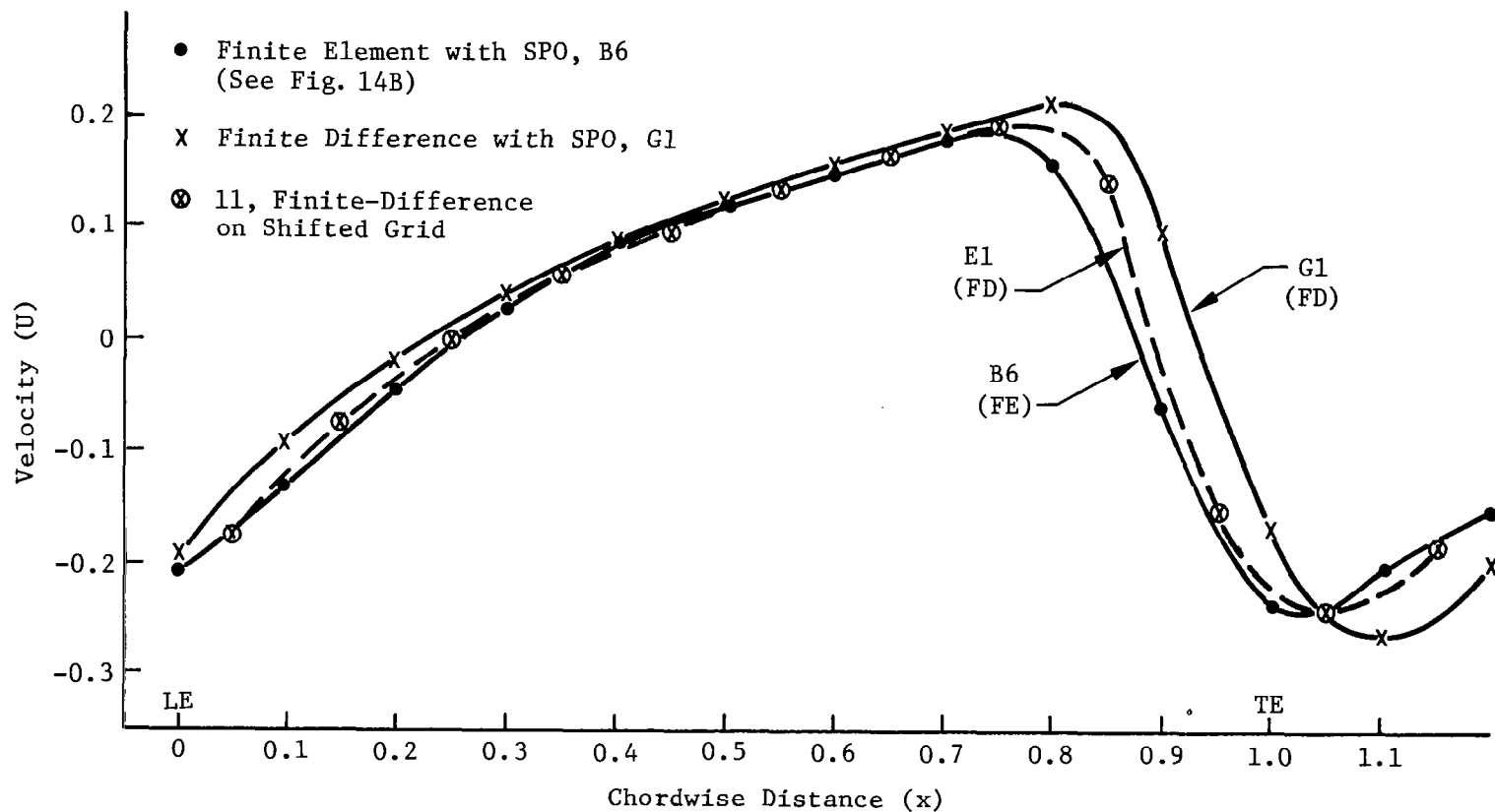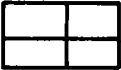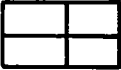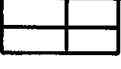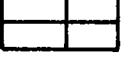
Figure 14A. Comparison Between Finite-Element and Finite-Difference Solutions
Using Shock-Point Operators

Case	Shock-Point Operator	Numerical Configuration Used
B6	Finite Element SPO	
C6	Finite Element SPO	
D6	Locally Normal SPO	
E6	Locally Normal SPO	

Note:. All Cases Gave Results Identical Within Three Significant Digits

Figure 14B. Identification of Finite-Element Solutions Using Shock-Point Operator
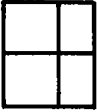
Case	Number of Iterations	Characteristics of Numerical Method		
A2	143			FE/FD Super.
B2	113			RE + AV
C2	190–Not Convergent Last Residual 9×10^{-5}			G
D2	190–Not Convergent Last Residual 2×10^{-4}			

Figure 15. Effect of Different Parabolic Blending Elements on Convergence
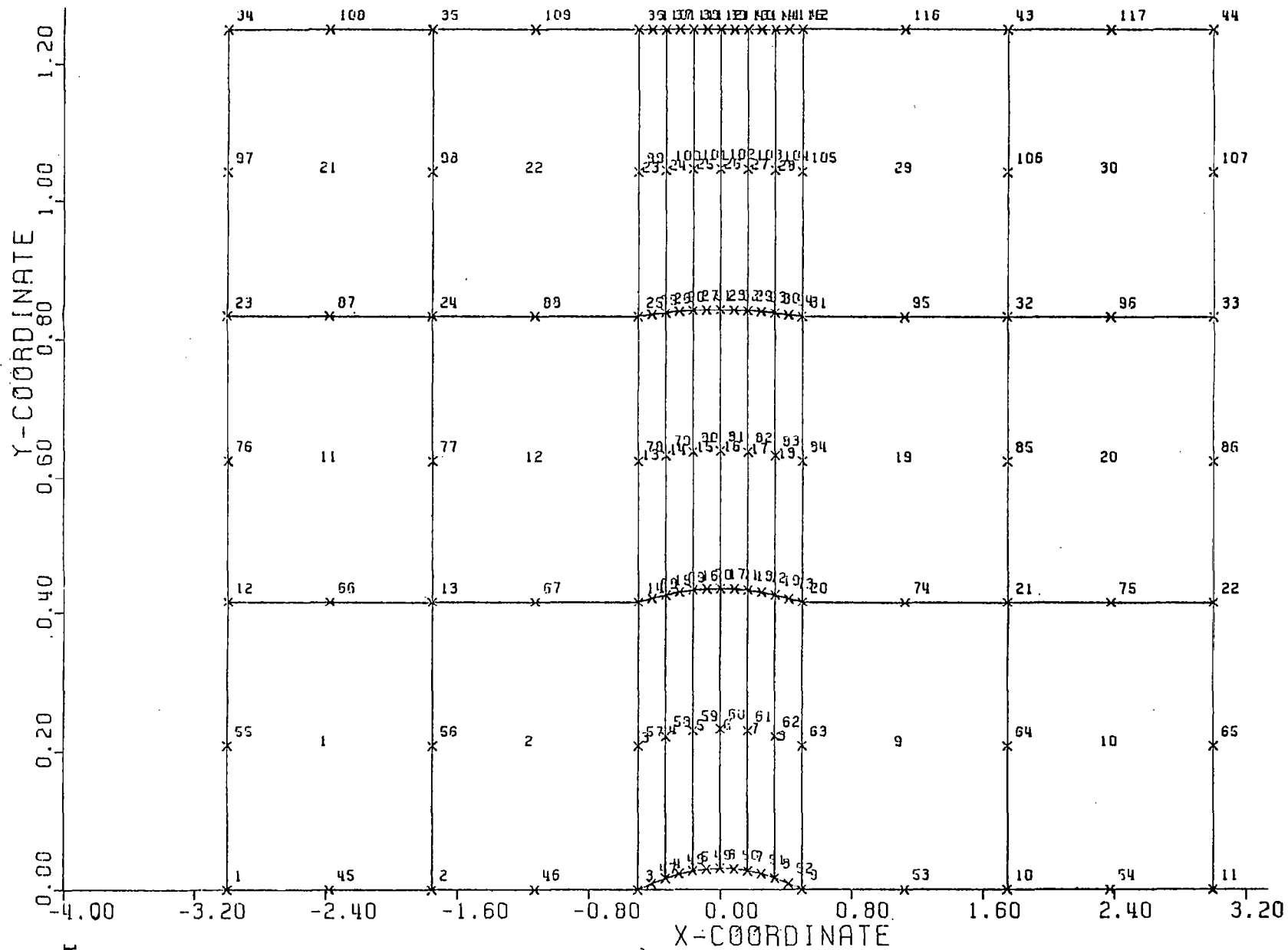in a Finite-Element Scheme

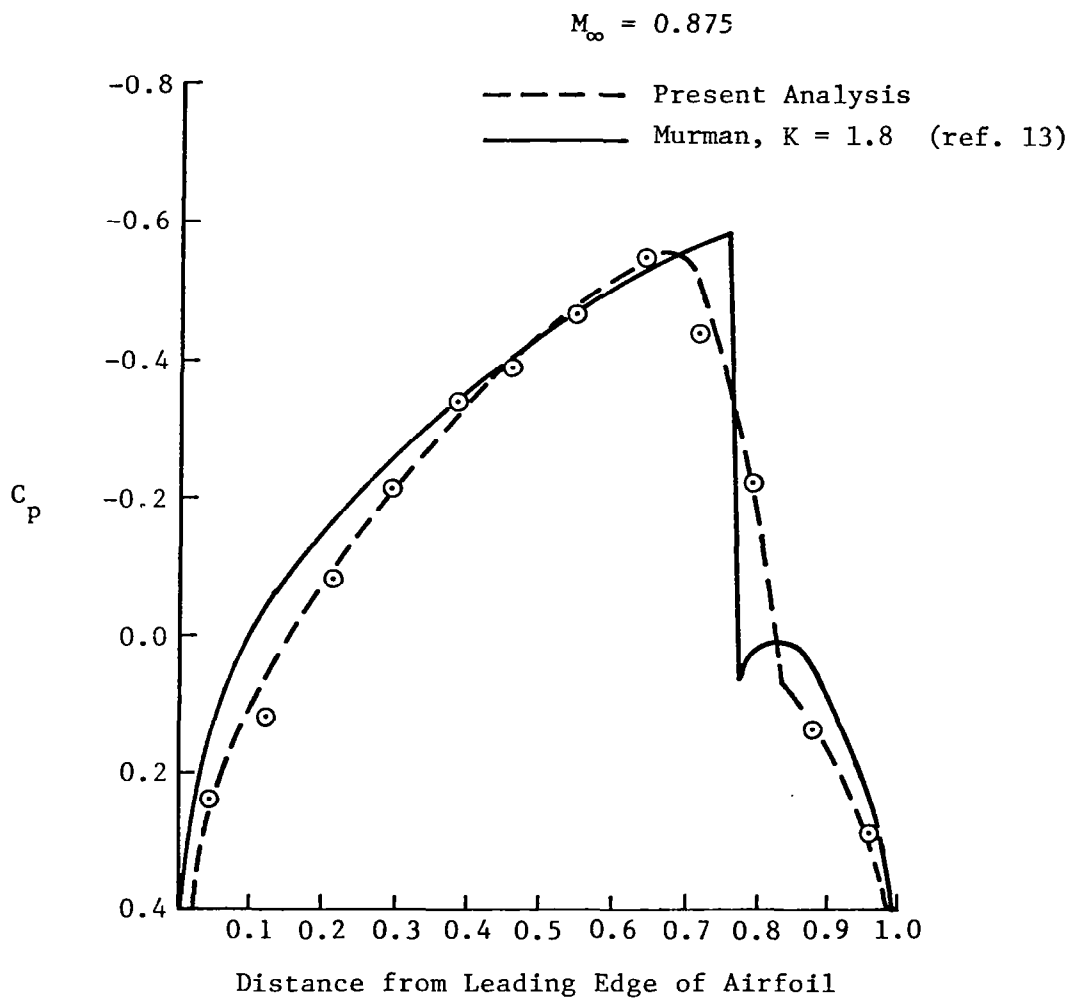Figure 16. Grid System Used For the Finite-Element Solution

Figure 17. Comparison Between the Finite-Element Solution of
Transonic Flow and the Finite-Difference Solution

1. Report No. NASA CR-3070	2. Government Accession No.	3. Recipient's Catalog No.
4. Title and Subtitle Numerical Computation of Transonic Flows by Finite-Element and Finite-Difference Methods		5. Report Date December 1978
		6. Performing Organization Code
7. Author(s) M. M. Hafez, L. C. Wellford, C. L. Merkle, and E. M. Murman		8. Performing Organization Report No.
		10. Work Unit No.
9. Performing Organization Name and Address Flow Research Company 21414 68th Avenue South Kent, Washington 98031		11. Contract or Grant No. NAS1-14246
		13. Type of Report and Period Covered Contractor Report
12. Sponsoring Agency Name and Address National Aeronautics and Space Administration Washington, DC 20546		14. Sponsoring Agency Code

15. Supplementary Notes
Langley Technical Monitor: Jerry C. South, Jr. Topical report.

16. Abstract

This report contains our studies on applications of the finite-element approach to transonic flow calculations. Different discretization techniques of the differential equations and boundary conditions are compared; finite-element analogs of Murman's mixed-type finite-difference operators for small-disturbance formulations are constructed; and the time-dependent approach (using finite differences in time and finite elements in space) is examined.

17. Key Words (Suggested by Author(s)) Transonic flow Aerodynamics Artificial viscosity	18. Distribution Statement Unclassified - Unlimited Subject Category 02

19. Security Classif. (of this report) Unclassified	20. Security Classif. (of this page) Unclassified	21. No. of Pages 122	22. Price* $6.50